Chapter 1
Introduction

The Earth is a living body. Its soul is its ability to grow. This soul, which also provides the Earth with its bodily warmth, is located in the inner fires of the Earth, which emerge at several places as baths, sulfur mines or volcanoes. Its flesh is the soil, its bones are the strata of rock, its cartilage is the tufa, its blood is the underground streams, the reservoir of blood around its heart is the ocean, the systole and diastole of the blood in the arteries and veins appear on the Earth as the rising and sinking of the oceans.

—Leonardo da Vinci (*Codex Leicester*, 1506–1510)

In *Codex Leicester* [61], da Vinci (see Sect. F.1 for a biography) drew the analogy between the Earth and the human body, to argue that Earth too, is a living body. He compared soils, rocks, and tufa (volcanic rock composed of fused detritus) to flesh, bones, cartilages, heart, arteries, and veins. We may ask, what do these materials have in common? They are all porous materials, that is, solid materials containing void space (pores) in them. Particularly, the pores can be occupied by a fluid, such be water, air, oil, methane gas, blood, body fluid, or a mixture of these.

This book is dedicated to the study of mechanics of porous materials, especially those infiltrated by a fluid. Porous materials can be found in nature as inanimate objects such as sand, soil, and rock, as living bodies such as plant tissue and animal and human flesh and bones, or as man-made materials for various industry or biomedical applications. These materials can look much different in their appearances due to their origin, but the underlying physical principles governing their mechanical behaviors can be the same. We are interested in the static and dynamic responses of these materials subject to mechanical as well as other type of forces, such as those of thermal and chemical origin. These studies are generally known as *poromechanics*.[1]

The modeling of a full range of porous material responses, ranging from quasi-static to dynamic, from linear to nonlinear, and from partial uncoupling to full coupling, can be complex and unwieldy. The goal of this book is limited. It focuses

[1]The term "poromechanics" was first created for the Biot Conference on Poromechanics [242].

A.H.-D. Cheng, *Poroelasticity*, Theory and Applications of Transport in Porous Media 27, DOI 10.1007/978-3-319-25202-5_1

largely on the linear theories, known as *poroelasticity*,[2] as in the linear theory of elasticity and Darcy flow; hence the book is of an introductory nature.

1.1 Porous Material

Porous material takes many shapes and forms. It can be a granular material, or a porous solid. Figure 1.1a shows a *granular material* as a pile of sand, which is a collection of particles of quartz, feldspar, mica, and other minerals of various sizes, ranging from 0.1 to 1 mm. Due to the irregular shape and random packing, a large percentage of the space is void, into which a fluid can penetrate and flow freely.

Figure 1.1b displays a section of sandstone under microscope. Sandstones are sand particles cemented together by calcite, clay and silica during the geological processes of sedimentation and compaction by overburden pressure. Unlike loose sand, sandstone is a *porous solid*; that is, a connected solid material containing pore space in it, shown in the figure as the areas without feature. The size of the pores for this sandstone is about 0.1 mm, and fluid can reside in it. In fact, rock can contain so much fluid such that it can be a water bearing and transmitting formation, known as *aquifer* in groundwater hydrology, or as an oil or gas bearing formation, called reservoir rocks in petroleum engineering.

Figure 1.1c shows a pumice, a volcanic rock. It contains large pores of millimeter or even centimeter sizes. The pores are formed by gas bubbles from exsolving volatiles during the cooling of lava. Figure 1.1d shows an outcrop of a fractured rock formation. Rock fractures can be caused by weathering or the change of underground stress environment. Fractured rock formations can be highly permeable. Even though the rock itself may not conduct water, a few large connected fractures can transmit a large quantity of water, and sometimes become the most productive aquifer.

The above are geomaterials occurring in nature. Porous materials can be manufactured. Concrete is a material used for the construction of buildings, roadways and ports by Romans since 2000 years ago. Concrete has relatively low porosity. Figure 1.1e however demonstrates a *pervious concrete* [266] with large porosity. The cement paste of this concrete is much reduced in order to create a large amount of interconnected pore space, yet it needs to be in sufficient amount to retain a large portion of its strength. Pavement made from this type of concrete can permeate and store water to reduce the surface runoff in the event of a storm.

Another artificial material is the ubiquitous polyurethane foam, seen under a microscope in Fig. 1.1f. The foam is lightweight and possesses good sound proofing, thermal insulating, and shock absorbing properties. Its structure can be open-cell or closed-cell. Figure 1.1f shows a cross section of a closed-cell foam. Figure 1.1g shows a *foam metal*, also known as structural foam. It can be created from various

[2]The term "poroelasticity" was first used by Deresiewicz and Skalak [69].

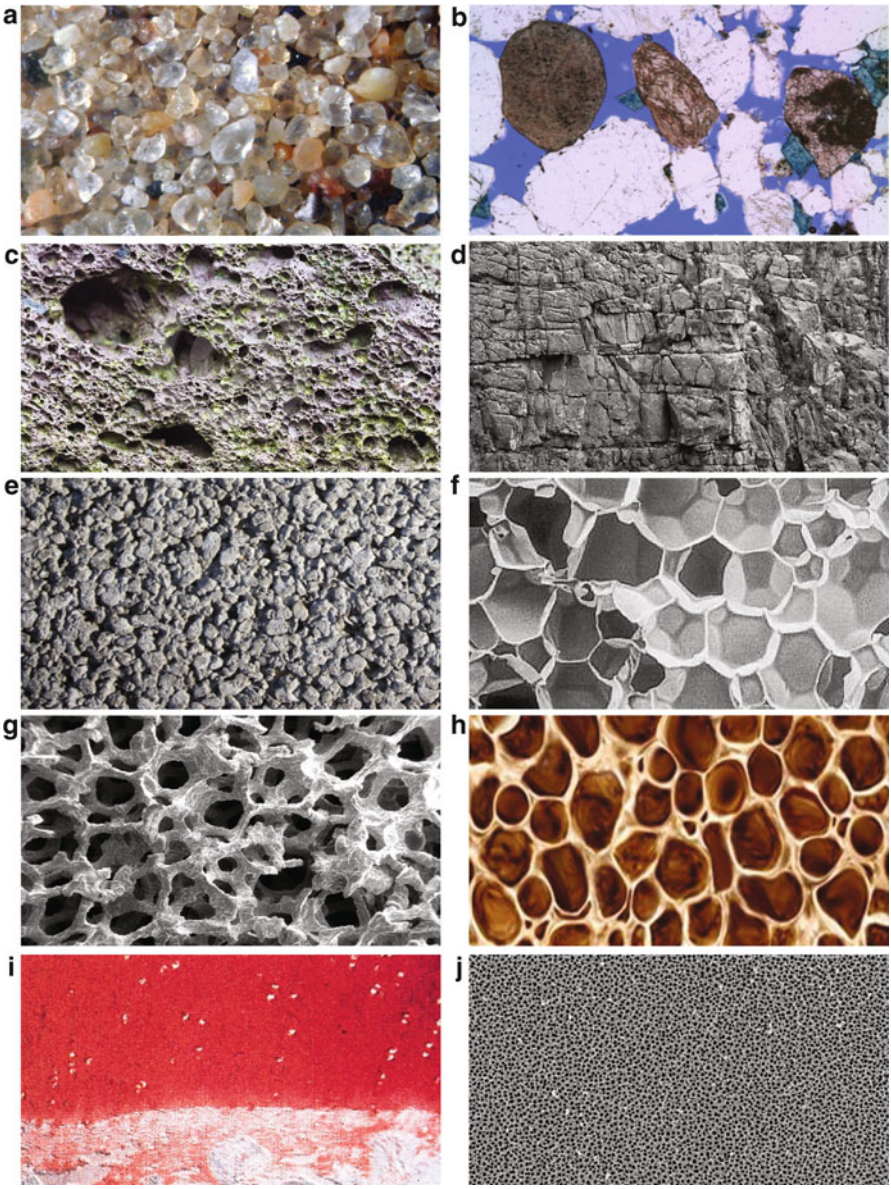

Fig. 1.1 Various porous materials. (**a**) Sand. (**b**) Sandstone. (**c**) Volcanic rock. (**d**) Fractured rock. (**e**) Pervious concrete. (**f**) Polyurethane foam. (**g**) Metal foam. (**h**) Bone with osteoporosis. (**i**) Articular cartilage. (**j**) Nanoporous alumina

metallic, glass, and carbon materials. It also can have closed or open cell structure. The one shown in the figure is open-cell. Such material is light weight and can be used for various purposes such as impact energy absorption, vibration damping, thermal and sound insulation, catalyst support, and metal and gas filtration [8].

Biological materials are typically porous. Figure 1.1h gives the cross section of a human bone. The pores of a living bone are filled with marrow. When the porosity of the bone increases for reasons such as aging or calcium deficiency, it leads to the disease called osteoporosis (means porous bone) [222]. The bone cross section in Fig. 1.1h is in fact a diseased bone with loss of bone mass. Figure 1.1i shows a healthy articular cartilage that lines the joint between two bones. The cartilage is a soft and porous material imbibed with fluid [170]. The viscous motion of fluid in the pores acts as a damper for shock loading. When the cartilage is compressed, fluid oozes out to provide a film of lubrication to reduce friction. Also, since the cartilage does not contain blood vessel, it relies on the squeezing motion of the fluid to bring nutrient to the cells. Hence the design and manufacturing of an artificial articular cartilage needs to take some of the above mechanisms into consideration [179, 180].

As observed above, pore space comes in various sizes, and in fact, pores can be as small as nano size. Nanoporous materials abound in nature, both in biological systems and in natural minerals. By definition, nanopores are of the size between 1 to 100 nm. Nanoporous solids have been made out of a wide variety of substances, including carbon, silicon, silicates, various polymers, ceramics, metals, metallic minerals, and organic materials [154]. Figure 1.1j shows the scanning electron micrograph of a nanoporous alumina membrane. Like the foam materials discussed above, the structure of nanoporous material can be open-cell, or closed-cell. In functional applications, open-cell porous materials are needed for adsorption, catalysis, sensing, separation, and filtration; and closed-cell materials are useful in acoustic, thermal insulation, and lightweight structural applications.

1.2 Physical Mechanism

Before a formal construction of the mathematical theory of poroelasticity, it is important to understand the basic mechanics of a fluid infiltrated porous material through *physical intuition*. To reflect on this view, we shall quote Maurice A. Biot (see Sect. F.14 for a biography), generally recognized as the "father of poroelasticity", from his acceptance speech of the Timoshenko Medal [22].

First, Biot expressed the honor of being associated with the name of Timoshenko, the great *Engineer and Scientist*. He praised Timoshenko's "*tradition of clarity, simplicity, intuitive understanding, unpretentious depth, and a shunning of the irrelevant*". Biot continued to say,

> *There is, of course, no merit in sophistication for its own sake. . . . We should not overlook the importance of simplicity combined with depth of understanding, not only for its cultural value, but as a technological tool. It leads to quantitative predictions without laborious and costly calculations; it suggests new inventions and simple solutions of engineering problems. . . . Deeper physical insight combined with theoretical simplicity provides the short-*

cuts leading immediately to the core of extremely complex problems and to straightforward solutions. This cannot be achieved by methods which are sophisticated and ponderous even in simple cases. The process of thought which is involved here may be described as cutting through the scientific red tape and bypassing the slow grinding mills of formal scientific knowledge. Of course, formal knowledge is essential but, as for everything in life, the truth involves a matter of balance. . . . it is essential to the make-up of a competent engineer.

It is in this spirit of "cut the red tape" of mathematical sophistication that in the sections to follow we shall discuss the mechanical responses of fluid infiltrated porous material by directly appealing to physical intuition.

1.2.1 Drained and Undrained Responses

For a fluid infiltrated porous material, its mechanical strength resisting compression is derived from three different sources. It is somewhat obvious that the rigidity of the solid and the fluid both contribute to the strength of material. It may be less obvious that the pore space, either carved in a piece of solid (porous solid), or in the intergranular space of stacked particles (granular material), has a strength that is dependent on the size, shape, orientation, and distribution of the pores.

By assigning an (apparent) strength to the pore space, which is a void, we are having in mind a composite material that various components contribute to the overall strength according to their volume fraction. The strength of the pore space is obviously smaller than the bounding solid that creates it, such that it weakens the material comparing to one that is totally solid without void. The strongest pore is that of spherical shape, with its strength characterized by the shear modulus of the solid and the porosity, and the weakest is a slit [59]. In fact if the slit has its orientation perpendicular to the applied stress direction, it readily closes offering no strength at all.

For granular materials, the major contribution of compressibility (inverse of rigidity) comes from the fluid and the pore structure, and not from the solid. For example, consider a pile of loose sand without fluid in it. We can make the sand particles (largely quartz) as rigid as they can be, yet they have little effect on the strength of the sand pile, which is rather weak subjected to compression. The strength of a granular material is largely determined by the denseness of the packing of the particles, not by the solid made of it. Fluid in liquid phase, on the other hand, can play an important part, particularly when it is trapped in the pores. In this subsection, we shall discuss the contribution of fluid in the rigidity of porous material under drained and undrained conditions.

Drained and undrained conditions are well-known concept in soil mechanics [146, 239]. Consider a porous solid with connected interstitial space that is saturated with a liquid. We can wrap this specimen in an impermeable but flexible membrane, and subject it to an all-around incremental compressive stress of magnitude ΔP. If we insert a tube through the membrane to reach the inside of the specimen, we can measure a pore pressure rise Δp. This experimental setup is called *undrained test* because the fluid is prevented from leaving the porous frame by the sealing membrane.

In a different experimental setup, we can leave the surface of the specimen exposed to atmosphere; or, we can utilize the tube inserted into the wrapped specimen and open its end to the atmosphere. In either of the above setup, fluid can flow out of the specimen. The flow process will continue, until everywhere in the specimen the pressure becomes equal to the atmospheric pressure, and $\Delta p = 0$. When a measurement is conducted in this state, it is called a *drained test*.

In both tests, we can measure the volumetric deformation of the specimen ΔV and compare it to the original volume V. The stiffness of the porous material can be characterized by the ratio of the applied load ΔP to the percentage change of volume $\Delta V/V$, known as volumetric strain. Following the concept of solid mechanics [93, 246], we can define a *material constant* characterizing the stiffness against volumetric deformation. For the drained test, we define

$$K = -\left.\frac{\Delta P}{\Delta V/V}\right|_{\text{drained}} \tag{1.1}$$

where K is called *drained bulk modulus*. (In the above, a negative sign is present because a positive compressive stress causes a decrease in volume.) Similarly, we can define an *undrained bulk modulus* K_u as

$$K_u = -\left.\frac{\Delta P}{\Delta V/V}\right|_{\text{undrained}} \tag{1.2}$$

In the following, we shall discuss the physical significance of these material constants.

For the drained test, the fluid is equilibrated with the atmospheric pressure, so it does not participate in the load bearing process. The drained bulk modulus K is then a measure of the stiffness of the *porous solid frame* without fluid. By porous solid frame we refer to the spatial structure consisting of the solid, as well as the enclosed voids (pores). When a frame is deformed, the reduction in volume is contributed both by the compression of the solid phase and by the compaction of empty space due to the structural rearrangement of the frame.

We may partition the total volume of the specimen V into two parts, a solid volume V_s, and a pore volume V_p, such that $V = V_s + V_p$. Then the change of total volume ΔV can also be partitioned into a solid and a pore part, such that $\Delta V = \Delta V_s + \Delta V_p$. If we consider that each part has its own stiffness against deformation, we then define these two apparent bulk moduli, respectively for the solid and the pore space, as

$$K_1 = -\frac{\Delta P}{\Delta V_s/V} \tag{1.3}$$

$$K_2 = -\frac{\Delta P}{\Delta V_p/V} \tag{1.4}$$

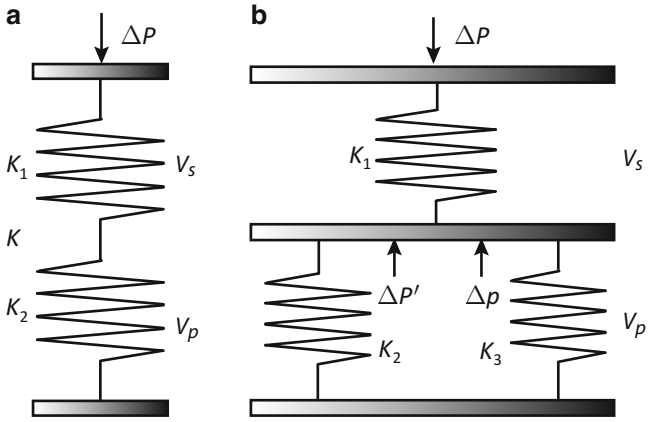

Fig. 1.2 Spring analogy: (**a**) Series springs for drained bulk modulus, and (**b**) Parallel springs for undrained bulk modulus

Utilizing the above, we can then express

$$\frac{\Delta V}{V} = \frac{\Delta V_s}{V} + \frac{\Delta V_p}{V} = -\Delta P \left(\frac{1}{K_1} + \frac{1}{K_2} \right) \tag{1.5}$$

Comparing with (1.1), it is apparent that

$$\frac{1}{K} = \frac{1}{K_1} + \frac{1}{K_2} \tag{1.6}$$

The above relation is similar to finding the equivalent spring constant of two coil springs arranged in a series. We hence can draw an analogy and present the relation among the rigidity of solid grain K_1, and of porous structure K_2, and the apparent rigidity of the frame K, as the series springs shown in Fig. 1.2a. If we consider a granular material, such as sand, with highly rigid solid grain (quartz), $K_1 \to \infty$, but weak porous structure, then the frame rigidity is dominated by the weak part, the pore structure, and the rigid solid has no effect on the value of K.

In Sect. 4.8.1, under an ideal porous medium condition (a porous medium made of homogeneous and isotropic solid material), we derive that

$$\frac{1}{K} = \frac{1}{K_s} + \frac{\phi}{K_p} \tag{1.7}$$

where K_s is the bulk modulus of the solid, K_p is the pore volume bulk modulus, and ϕ is porosity. Hence we confirm the series spring analogy.

Next, we examine the undrained condition in which the fluid is entrapped in the pores. When a load ΔP is applied and the pore volume is compressed, not only the porous structure, but also the entrapped fluid, will resist. If the former gives

a reaction stress $\Delta P'$ and the latter a pore pressure Δp, then $\Delta P = \Delta P' + \Delta p$. Particularly, the reaction stress provided by the pore structure, $\Delta P'$, is called an *effective stress*.

We may consider the above situation analogous to the parallel springs as shown in Fig. 1.2b. If we consider that $\Delta P'$ causes the pore volume to deform in the amount ΔV_p, with a bulk modulus K_2, and Δp causes the fluid volume to deform ΔV_f, with a bulk modulus K_3, then

$$K_2 = -\frac{\Delta P'}{\Delta V_p / V} \tag{1.8}$$

$$K_3 = -\frac{\Delta p}{\Delta V_f / V} \tag{1.9}$$

Summing the partial stresses $\Delta P'$ and Δp, and realizing that $\Delta V_f = \Delta V_p$ as the fluid occupies the pore space, we obtain

$$\Delta P = \Delta P' + \Delta p = -(K_2 + K_3)\frac{\Delta V_p}{V} \tag{1.10}$$

The above shows that we can define an equivalent bulk modulus

$$K_4 = K_2 + K_3 \tag{1.11}$$

just as the equivalent spring constant for parallel springs. However, we need to exercise some caution in the above argument. In order to arrive at a simple model, we have neglected an important effect that the pore pressure Δp can cause the solid volume V_s to deform too; so the actual model is more complex than the combined series-parallel spring system depicted in Fig. 1.2b.

Nevertheless, the above simplified model allows us to gain some basic physical understanding, and we may consider some limiting cases. For example, if the solid grains are relatively rigid, $K_1 \to \infty$, then the compressibility of the undrained material is dominated by the parallel springs system with bulk modulus K_4. In fact, in Sect. 4.8.2, it is demonstrated that for the special case that $K_s \to \infty$, the undrained bulk modulus is given by

$$K_u = K + \frac{K_f}{\phi} \tag{1.12}$$

The above equation confirms our intuitive model based on parallel spring analogy. Also, as the undrained bulk modulus is the sum of the drained bulk modulus and fluid bulk modulus, it is obvious that $K_u > K$. The above result shows that a porous material is stiffer under undrained condition than drained, as both the solid frame and the fluid are reacting to the load. Furthermore, we can consider the case that the fluid is much less compressible than the porous medium frame, and in fact incompressible, $K_f \to \infty$. In this case, the entire system is incompressible under undrained condition, which is the model for clay consolidation considered by Terzaghi [235, 237].

Tables 3.1 and 3.2 give a list of typical values of K, K_u, K_p, K_s, and K_f for a range of natural and man-made materials.

1.2.2 Time and Length Scale

In the above section we have described the undrained condition as one that is created by wrapping the sample in an impermeable membrane. This is in fact not a necessary condition for the undrained behavior. Fluid is a *viscous* material such that it takes a finite amount of time for fluid to move a finite distance. If a loading is instantly applied, fluid is trapped in the pore space even if the sample surface is open for drainage. Hence a porous material is in an undrained state responding to an instantly, or rapidly, applied load, whether its surface is sealed or exposed to atmosphere.

Given time, however, a small amount of the fluid will be expelled from the solid frame if the specimen is not completely sealed. This allows the fluid to expand, thus giving relief to the pressure. Eventually the pressure will equilibrate with the ambient or atmospheric pressure, and the state is referred to as drained. The stiffness of a porous material therefore gives the appearance of time dependency—it is stiffer (undrained) at small times, and continues to soften (drained) at large times.

In the above, when we refer to small or large time, we do not mean absolute time. Unlike some solid materials that exhibit time dependent behavior (viscoelasticity), which is a material property with absolute time, this time is relative to the *time scale* for the completion of the physical process of a given problem. This time scale is dependent not only on the solid and fluid material properties, but also on the size and geometry of a particular problem.

Karl Terzaghi (see Sect. F.12 for a biography) was the first to model the creep phenomenon of saturated clay as a *soil consolidation* process [234, 237]. He recognized that when a uniform surcharge is suddenly applied to the top of a clay layer, the soil is initially undrained and an initial excess pore water pressure p_o is generated. The excess pore water pressure will dissipate through the top surface following a one-dimensional diffusion equation

$$\frac{\partial p}{\partial t} - c\,\frac{\partial^2 p}{\partial x^2} = 0 \tag{1.13}$$

where c is a *consolidation coefficient* with dimension of [L^2/T], which is a combined property of the permeability of the clay and the elasticity of the solid skeleton.

To obtain a solution that is independent of the physical dimensions of the problem, and of the magnitude of the loading, we can perform nondimensionalization to (1.13) by introducing a *characteristic length* L_c, and the dimensionless quantities

$$p^* = \frac{p}{p_o}, \quad x^* = \frac{x}{L_c}, \quad t^* = \frac{c\,t}{L_c^2} \tag{1.14}$$

to obtain

$$\frac{\partial p^*}{\partial t^*} - \frac{\partial^2 p^*}{\partial x^{*2}} = 0 \tag{1.15}$$

We observe that (1.15) is free from any material coefficient.

The definition of the dimensionless time in (1.14) suggests a *characteristic time* $t_c = L_c^2/c$, and $t^* = t/t_c$. For the consolidation problem, the characteristic length is the thickness of the layer, that is, the distance that the pressure relief wave front needs to travel to reach the farthest region of pore pressure buildup. The characteristic time t_c is then the time it takes for the layer to be significantly drained. With this definition, a *small time* is referred to as $t \ll t_c$, and a *large time* is $t \gg t_c$. It is of interest to note that t_c is dependent on both the material properties, and the physical size of the problem. Particularly, it is proportional to the square of the characteristic length of the problem.

The time scale and length scale can manifest themselves in many different ways. For example, consider a case of cyclic loading created by a vibrating machinery on top of a soil layer, with a stress that is sinusoidal in time $P = P_o \sin \omega t$. In this case, there exists a characteristic frequency $\omega_c = c/L_c^2$ for diffusion, such that if the vibration is at high frequency, $\omega \gg \omega_c$, the layer behaves as an undrained material, and at low frequency, $\omega \ll \omega_c$, the layer is characterized by the drained property.

Now consider the case of high frequency. Although the layer is generally undrained, there exists a region near the top where the soil is drained, enforced by the boundary condition. In this case, we find a characteristic length $\delta_\ell = \sqrt{c/\omega}$ such that within this distance, the soil is largely drained. This thickness δ_ℓ is called a *boundary layer thickness* [165], within which the diffusion process is important, and outside which the undrained elastic behavior dominates. (It should be noted that the discussion in this section is limited to the quasi-static poroelasticity, with diffusion effect only, and without the dynamic wave propagation effects.)

Or, we can consider a moving load. The moving load can be a wheel traveling at a speed v on the surface of a soil layer [35], a drilling bit advancing and excavating the material ahead of it [6], or a propagating fracture [49]. For the moving wheel, if the surface of the soil is drained, then there is a region directly underneath the wheel where the soil is largely drained. Farther away, however, the speed of the wheel can be too fast to allow time for the induced pore pressure to dissipate. A length scale near the wheel within which the soil is drained is characterized by $L_c = c/v$. When the velocity is faster, the region is smaller, and the overall material response is close to undrained. When the velocity is slower, the material approaches the drained behavior.

1.2.3 Skempton Pore Pressure Effect

Let us consider the undrained condition. As the fluid is trapped, it will resist a compressive confining stress of magnitude ΔP and give rise to a pore pressure

increment Δp. Generally speaking, we anticipate that Δp is smaller than the applied load, $0 \leq \Delta p \leq \Delta P$. Skempton [226] measured this pore pressure rise and defined the relation

$$\Delta p = B\Delta P \tag{1.16}$$

in which B is the *Skempton pore pressure coefficient B*. It is anticipated that $0 \leq B \leq 1$, though a value $B > 1$ is possible.

Equation 1.16 is defined in three dimensions, and

$$\Delta P = -\frac{\sigma_{xx} + \sigma_{yy} + \sigma_{zz}}{3} \tag{1.17}$$

is the average compressive stress, where σ_{xx}, σ_{yy}, and σ_{zz} are stress tensor components, defined *positive for tension*. Under *plane strain* condition, that is, the body is confined from movement in one of the spatial dimensions, say z, then we define on the x-y plane

$$\Delta P = -\frac{\sigma_{xx} + \sigma_{yy}}{2} \tag{1.18}$$

and find the following relation for the Skempton effect [42]

$$\Delta p = \frac{2B(1 + \nu_u)}{3}\Delta P \tag{1.19}$$

where ν_u is the *undrained Poisson ratio*. Furthermore, if the deformation is allowed in one dimension only, say x, and a load $\sigma_{xx} = -\Delta P$ is applied, then the uniaxial Skempton effect is characterized by this pressure rise

$$\Delta p = \frac{B(1 + \nu_u)}{3(1 - \nu_u)}\Delta P \tag{1.20}$$

The above proportionality constant is also called the *tidal efficiency* [126]

$$\gamma_{te} = \frac{\Delta p}{\Delta P} = \frac{B(1 + \nu_u)}{3(1 - \nu_u)} = \frac{3BK_u}{4G + 3K_u} \tag{1.21}$$

where G is shear modulus. It is a constant associated with the ratio of water level rise in water wells resulting from the rise of ocean tide, a phenomenon that will be discussed in Sect. 1.3.10.

Referring to the parallel spring analogy in Fig. 1.2b, it is easy to realize that the share of the reaction force between $\Delta P'$ and Δp is proportional to their respective spring constants K_2 and K_3; that is, the stiffer the spring is, the more load that spring

takes. Using (1.8) and (1.9) to eliminate the volume terms, and substituting in (1.10) for the total load ΔP, we find that

$$\frac{\Delta p}{\Delta P} = \frac{K_3}{K_2 + K_3} = \frac{K_3}{K_4} \tag{1.22}$$

Assuming that the solid constituent is incompressible, we can utilize the relation (1.12) and (1.16) to obtain

$$B = \frac{K_f}{\phi K + K_f} \tag{1.23}$$

which is presented as (4.166).

Based on the above relation, we can examine some limiting cases. If the stiffness of the skeleton is much smaller than that of fluid, $K \ll K_f$, which is the case for soil saturated with water, then the fluid is bearing most of the load. In the limit, we expect $\Delta p \to \Delta P$ and $B \to 1$. This is the case that Terzaghi [234] considered in the theory of soil consolidation. Indeed, the Terzaghi theory has the inherent assumption that both the fluid and the solid are incompressible as compared to the soil skeleton, such that $K_f/K \to \infty$ and $K_s/K \to \infty$, which in turn leads to the condition $K_u/K \to \infty$. Hence saturated clay is considered incompressible at the instant of loading. Another special case to consider is that the fluid is not a liquid, but a gas. As gas is highly compressible, $K \gg K_f$, and there is little or no pressure rise; hence $\Delta p \to 0$ and $B \to 0$.

A more curious case is that, if the solid is soft, and softer than the liquid occupying the pore space, then the pore pressure rise can be greater than the load applied; that is, $\Delta p > \Delta P$, and $B > 1$. Such situation can exist for polyurethane foam saturated with a liquid. In that case, the solid part is in effective tension. This effect is more difficult to visualize, but can indeed be predicted by the micromechanical analysis (see Sect. 4.8.5), and observed in laboratory. Typical values of B are given in Table 3.2, and we do see that B can be greater than 1.

1.2.4 Effective Stress for Volumetric Deformation

Consider a porous medium under drained condition. When there exists a confining compressive stress ΔP, it is obvious that the load is entirely supported by the solid, and a volumetric deformation ΔV will result. On the other hand, if the fluid is not drained and there is fluid pressure Δp above the ambient pressure, then the pore pressure will counteract the applied load ΔP, such that the effective load applied to the solid frame is reduced. In Sect. 1.2.1 we argued that such effective load is simply $\Delta P' = \Delta P - \Delta p$. This is however not true. As we have commented, in order to reach such relation, we neglected the solid compressibility by assuming $K_s \to \infty$. The question is, as the solid is compressible, and the pressure has an

effect of compressing the solid, what is the effective reduction of the load applied to the solid? In other words, what is the *effective stress* applied to solid frame that can correctly predict the deformation of the frame? We shall answer this question in this section.

Putting the above question into an equation, it becomes

$$\frac{\Delta V}{V} = -\frac{1}{K}(\Delta P - \alpha \Delta p) \tag{1.24}$$

in which the left hand side is the volumetric strain of the frame, K is the drained bulk modulus of the frame, and α is the coefficient in question. The coefficient α defines the weighted contribution of pore pressure to the load reduction, and is called the effective stress coefficient. It has the value between 0 and 1, where 0 means that the pore pressure has no effect on the load reduction, and 1 means it has the full effect.

Based on an extensive historical study, de Boer [63–65] called the attention to a controversy between Karl von Terzaghi, *father of soil mechanics*, and Paul Fillunger, *father of mixture theory*, on the correct form of the effective stress. According to de Boer, the controversy is still not settled [26, 66, 145].

Terzaghi was more an engineer than a theoretician. Based on his physical intuition and laboratory observation, Terzaghi [234, 236] proposed the following effective stress law (see a historical review by Skempton [227]),

$$\frac{\Delta V}{V} = -\frac{1}{K}(\Delta P - \Delta p) = -\frac{\Delta P'}{K} \tag{1.25}$$

where

$$\Delta P' = \Delta P - \Delta p \tag{1.26}$$

is the *Terzaghi effective stress*. The above effective stress law has been widely adopted in soil mechanics, as well as man-made materials such as concrete. Fillunger [86], on the other hand, was more theoretically oriented. He derived the following effective stress law based on the forerunner of modern day mixture theory [66],

$$\frac{\Delta V}{V} = -\frac{1}{K}(\Delta P - \phi \Delta p) \tag{1.27}$$

in which ϕ is the porosity. It should be mentioned that in arriving at the above results, both Terzaghi and Fillunger assumed that the solid constituent is incompressible [66], while the solid frame is compressible.

The two effective stress laws, (1.25) and (1.27), clearly do not agree. To find out which of the above is correct, we can subject these relations to a *thought experiment*. Let us consider an *ideal porous medium*; that is, a porous medium made of a homogeneous and isotropic solid [97]. We can submerse this porous specimen in a chamber filled with a fluid. If we raise the fluid pressure in the chamber by Δp,

it is clear that there is an incremental compressive stress applied to the specimen as $\Delta P = \Delta p$. If we wait long enough for the fluid pressure inside the porous medium to equilibrate with the chamber pressure, then the pore pressure rise is also Δp. This loading condition implies that the Terzaghi effective stress $\Delta P' = 0$.

Under this test condition, the entire solid surface that is in contact with the fluid, internal and external, is subjected to the same normal stress Δp. Due to the material homogeneity and isotropy, a simple elasticity solution shows that every point inside the solid is under uniform compression, and there is no shear stress. Since both Terzaghi and Fillunger consider the solid constituent as incompressible, the solid simply does not deform! This easily leads to the conclusion that $\Delta V = 0$, and that the Terzaghi effective stress law (1.25) is correct. Fillunger's equation (1.27), on the other hand, indicates that the frame will deform by the amount $\Delta V/V = -(1/K)(1-\phi)\Delta p$. This is certainly erroneous, and the error is the largest for small porosity materials.

In Sect. 1.1 we discussed two types of porous material, a granular material and a porous solid. For a granular material such as sand, shown in Fig. 1.1a, it is clear that the pore space is much more compressible than the individual sand particles; hence the *incompressible solid constituent* assumption used above is a reasonable one. For a porous solid with low porosity and spherical pores, however, the pore space is well protected, and its compressibility is comparable to that of the solid. In that case, the solid compressibility must be considered together with the pore compressibility; hence the Terzaghi's effective stress law needs to be modified.

Now let us consider the solid constituent as compressible and reexamine the above thought experiment. First, it is convenient to rewrite (1.24) into the following form:

$$\frac{\Delta V}{V} = -\frac{1}{K}\left[\Delta P' + (1-\alpha)\Delta p\right] \tag{1.28}$$

where P' is defined in (1.26). Under the present loading condition, $\Delta P' = 0$ and the above equation becomes

$$\frac{\Delta V}{V} = -\frac{1}{K}(1-\alpha)\Delta p \tag{1.29}$$

Hence we can directly relate the volume change of the specimen to the pressure change in the chamber.

Following the same argument as above, when the fluid pressure in the chamber is raised by Δp and the system reaches an equilibrium, the homogeneous and isotropic specimen is under uniform compression everywhere. As a consequence, the entire solid deforms in a geometrically similar fashion. This deformation will preserve not only the shapes of the solid, but also that of the pore space. This condition then leads to the following proportions

$$\frac{\Delta V_s}{V_s} = \frac{\Delta V_p}{V_p} = \frac{\Delta V}{V} \tag{1.30}$$

where V_s, V_p and V, as defined in Sect. 1.2.1, are the solid, the pore, and the total volume, respectively. The solid deformation is given by

$$\frac{\Delta V_s}{V_s} = -\frac{\Delta p}{K_s} \tag{1.31}$$

where K_s is the bulk modulus of the solid. Substituting (1.30) and (1.31) into (1.29), we clearly see that in order for the effective stress law to pass this thought experiment, we must have

$$\alpha = 1 - \frac{K}{K_s} \tag{1.32}$$

This is indeed what proposed by Biot [16, 23]. We hence define the *Biot effective stress* $\Delta P''$ as

$$\Delta P'' = \Delta P - \alpha \Delta p \tag{1.33}$$

such that

$$\frac{\Delta V}{V} = -\frac{\Delta P''}{K} \tag{1.34}$$

which is the correct effective stress law. The coefficient α is referred to as the *Biot effective stress coefficient*. We also notice that the *incompressible constituent model* is given by $K_s \to \infty$, which means that $\alpha = 1$, and (1.24) reduces to (1.25). We then conclude that the Terzaghi effective stress law is a special case of the Biot effective stress law. In the other limit, it can be proven that the composite bulk modulus of the porous frame (solid and pores) is always smaller than that of the solid, $K \leq K_s$, known as the Hashin-Shtrikman bound [111], and $K \to K_s$ only if $\phi \to 0$ [155]. Hence $\alpha = 0$ for a pure solid, which is an obvious conclusion. Typical values of α for a range of different materials are given in Table 3.2.

It may be of interest to also examine the result derived from the modern mixture theory [26, 145, 231]:

$$\begin{aligned} \frac{\Delta V}{V} &= -\frac{1}{K}\left\{\Delta P - \left[1 - (1-\phi)\frac{K}{K_s}\right]\Delta p\right\} \\ &= -\frac{1}{K}\left[\Delta P - (\alpha + \phi - \alpha\phi)\Delta p\right] \end{aligned} \tag{1.35}$$

The above effective stress law approaches that of Biot's if $\phi \to 0$. But this law obviously does not pass the above thought experiment, so one needs to be very careful about its use.

We should note that the above presentation is based on the ideal porous medium assumption. However, one only needs to take a look at the material of sand, such as

the one shown in Fig. 1.1a, to realize that porous materials are hardly homogeneous at the grain size scale. For a real porous medium, it can be shown that the Biot effective stress law (1.24) is still valid; but the solid bulk modulus K_s appearing in (1.32) needs to be interpreted differently. This more general porous medium theory is presented in Chaps. 3 and 4.

1.2.5 Effective Stress for Pore Collapse

When a porous material is subjected to a large deformation, leading to the failure of the material, it is observed that the threshold for failure is predicted not directly by the total stress applied, but by a certain difference between the total compressive stress and the pore pressure—in other words, an effective stress. In the above section we have demonstrated that the volumetric deformation of poroelastic material is related to the Biot effective stress. For failure, however, experimental evidences have shown that the threshold is largely associated with the Terzaghi effective stress, and not the Biot effective stress [78, 96, 109]. This phenomenon can be explained as follows.

For a porous material, the strength of the pore structure is always weaker than the strength of the solid that surrounds it. A theoretical proof of this is called the Hashin-Shtrikman bound [111], as mentioned in the above section. When a porous material fails, either by compression or shear, it is likely that the pore structure is destroyed first, known as *pore collapse* [263], before the solid constituent fails. Furthermore, we can argue that it is not the change of pore volume alone, but the *disproportional* changes of pore volume versus solid volume that will cause the pore structure to fail. To visualize this, let us again construct a thought experiment using the example of an ideal porous medium submersed in a fluid chamber. As discussed in the preceding section, when the fluid pressure in the chamber is raised, the porous medium deforms in a geometric similar fashion. In other words, the pore space is reduced in the same proportion as the solid constituent, and its shape is preserved. When the chamber pressure is continuously increased, the porous material will not fail by pore collapse, until it reaches a point that the solid constituent fails. From the above description, it is clear that the failure is more strongly related to the relative change between the pore volume and the total volume, that is, the change in porosity, than the change in pore volume or total volume alone.

From this reasoning, we need to construct the constitutive law between the change of porosity, $\Delta\phi$, and the applied stresses, ΔP and Δp. We may assume that there exists a linear relation,

$$\Delta\phi = a\,\Delta P - b\,\Delta p \tag{1.36}$$

Or, we can put that relation in a different form

$$\Delta\phi = a\,\Delta P' - b'\,\Delta p \tag{1.37}$$

where $\Delta P'$ is the Terzaghi effective stress. If we subject an ideal porous medium to the above-stated experiment, then the loading conditions gives $\Delta P' = 0$. Porosity is defined as

$$\phi = \frac{V_p}{V} \tag{1.38}$$

and its variation is

$$\Delta\phi = \Delta\left(\frac{V_p}{V}\right) = \frac{V\Delta V_p - V_p\Delta V}{V^2} \tag{1.39}$$

Utilizing (1.30), it is easy to show that under this test condition, we must have $\Delta\phi = 0$. We hence conclude that $b' = 0$, and (1.37) becomes

$$\Delta\phi = a\,\Delta P' \tag{1.40}$$

Hence the porosity change is dependent on the Terzaghi effective stress only. In Sect. 3.2, we shall demonstrate such constitutive law

$$\frac{\Delta\phi}{1-\phi} = -\frac{\Delta P'}{K_\varphi} \tag{1.41}$$

where K_φ is the *bulk modulus of porosity*. We therefore confirm the laboratory observation that the failure of porous material is largely associated with the Terzaghi effective stress.

1.2.6 Fluid Storage

In groundwater and petroleum engineering applications, fluid can be extracted from water and oil bearing formations by lowering the fluid pressure in a cavity to induce a porous medium flow into it for collection (production). The effect of lowering the fluid pressure in the porous medium causes the fluid to expand and the formation to compact, thus releasing the fluid.

In a reverse application, fluid can be injected into the formation. For groundwater applications, it can be the recharging of treated waste water for later reclamation and reuse; or, for petroleum engineering, for the disposal of oil field brine. The re-injection of fluid into the formation can reverse the trend of land subsidence caused by the past excessive extraction. In present day, to combat the carbon dioxide greenhouse effect, the capturing of CO_2 emission and the *geoengineering* (also called *climate engineering*) of storing it in deep underground formation has been used as a climate remediation technique [85]. With these applications, it is of interest to learn about the fluid storage capacity of a porous medium.

The storage capacity of a porous medium can be quantified by the definition of a *storage coefficient*, given as the volume of fluid stored into or extracted from a unit volume of porous medium per unit increase or decrease of fluid pressure. Depending on the constraint imposed on the porous medium during measurement, two storage coefficients can be defined: S_e is a storage coefficient measured under the condition of constant sample volume (constant strain), and S_σ is measured under constant confining stress.

There are several ways that fluid can be accommodated into or expelled from the porous frame. One way is for the solid frame to expand or to compact; the second is for the solid constituent to dilate or to contract; and the third way is for fluid itself to be compressed or to expand. Hence we expect the storage coefficients to be dependent on the three bulk moduli, K, K_s, and K_f, as well as the porosity. Indeed, it is demonstrated in Sects. 2.4.4 and 3.2 that

$$S_e = \frac{1}{M} = \frac{\phi}{K_f} + \frac{1-\phi}{K_s} - \frac{K}{K_s^2} \tag{1.42}$$

$$S_\sigma = C = \frac{\phi}{K_f} + \frac{1}{K} - \frac{1+\phi}{K_s} \tag{1.43}$$

where M and C are poroelastic constitutive constants.

Typically, the solid constituent is less compressible than both the fluid or the frame, $K_s \gg (K, K_f)$; hence (1.42) and (1.43) can be approximated as

$$S_e = \frac{\phi}{K_f} \tag{1.44}$$

$$S_\sigma = \frac{\phi}{K_f} + \frac{1}{K} \tag{1.45}$$

Another storage coefficient of interest is that used in groundwater aquifer theory [13, 41]. The specific storativity S_s is defined as the volume of water released from storage per unit volume of porous medium per unit decline of piezometric head under uniaxial strain and constant overburden condition [13]. Or, adjusting the above definition from per unit decline of head to per unit decline of pressure, we obtain the constant stress uniaxial storage coefficient S as

$$S = \frac{S_s}{\gamma_f} = \frac{\phi}{K_f} + \frac{3}{3K + 2G} \tag{1.46}$$

where γ_f is the specific weight of water.

1.2.7 Thermoelasticity Analogy

The *coupled theory of thermoelasticity* was established by Biot [17] on the basis of irreversible thermodynamic processes [177]. In the same paper, Biot also

demonstrated the mathematical equivalence between the governing equations of poroelasticity and thermoelasticity.

For poroelasticity, the following governing equations are presented in Sect. 6.3:

$$\mu\nabla^2\vec{u} + (\lambda + \mu)\,\nabla e - \alpha\nabla p = 0 \tag{1.47}$$

$$\frac{\partial p}{\partial t} - \kappa M\nabla^2 p = -\alpha M\frac{\partial e}{\partial t} \tag{1.48}$$

where $\vec{u}$ is the displacement vector, $e = \nabla\cdot\vec{u}$ is the volumetric strain (dilatation), λ and μ are Lamé constants, κ is the permeability coefficient, and $1/M = S_e$ as defined in the above section. For thermoelasticity, the governing equations are [17, 20, 177]

$$\mu\nabla^2\vec{u} + (\lambda + \mu)\,\nabla e - \alpha_T\nabla T = 0 \tag{1.49}$$

$$\frac{\partial T}{\partial t} - \frac{k_T}{c_v}\nabla^2 T = -\frac{\alpha_T\mathcal{T}_o}{c_v}\frac{\partial e}{\partial t} \tag{1.50}$$

where T is the temperature increment from a reference temperature $\mathcal{T}_o$, k_T is the *thermal conductivity*, c_v is the *specific heat at constant strain*, and

$$\alpha_T = (3\lambda + 2\mu)\,\beta_l \tag{1.51}$$

is a thermoelastic constitutive constant, with β_l the *coefficient of linear thermal expansion*. Comparing the two sets of equations, (1.47) and (1.48) with (1.49) and (1.50), we observe the mathematical equivalence between pore pressure and temperature $p \leftrightarrow T$, and the coefficients $\alpha \leftrightarrow \alpha_T$, $\kappa \leftrightarrow k_T/\mathcal{T}_o$, and $M \leftrightarrow \mathcal{T}_o/c_v$ [43, 98, 176].

For thermoelasticity, it can be shown that the *entropy density* s satisfies the diffusion equation [17]

$$\frac{\partial s}{\partial t} - \frac{k_T(\lambda + 2\mu)}{c_v(\lambda + 2\mu + \alpha_T^2\mathcal{T}_o/c_v)}\nabla^2 s = 0 \tag{1.52}$$

which can be compared with the diffusion equation for poroelasticity,

$$\frac{\partial\zeta}{\partial t} - c\nabla^2\zeta = 0 \tag{1.53}$$

where ζ is the *variation in fluid content*, defined as the amount of fluid volume entering the solid frame per unit volume of solid frame, and c is the consolidation coefficient, given by

$$c = \frac{\kappa M(\lambda + 2\mu)}{\lambda + 2\mu + \alpha^2 M} \tag{1.54}$$

Here we see the analogy $\zeta \leftrightarrow s$. In the following, we shall use the above established analogies to visualize a few poroelastic effects.

Envision a solid body whose sides are not constrained by forces and are free to move. If the temperature of the solid is raised, it will expand, a phenomenon known as *thermal expansion*. Similarly, given a poroelastic body that is unconstrained, if the pore pressure inside the body is raised by injecting fluid into it, the frame will likewise expand. This can be viewed as a mathematical analogy with thermoelasticity; or, we may consider this as a result of effective stress. As the total stress is zero, a positive pore pressure gives rise to a negative effective compressive stress; that is, the body is under effective tension, hence it expands.

Consider a different situation. The solid body is constrained from movement on all sides and the temperature is raised. A *thermal stress* develops, sets the body into compression. Similarly, for poroelasticity, when fluid is injected into a constrained body to raise its pressure, a compressive stress is observed.

In Sect. 1.2.3 we discussed that when an poroelastic body is suddenly subjected to a compressive confining stress, a pore pressure rise is observed, known as the Skempton pore pressure effect. By analogy, when an elastic solid is suddenly compressed, we anticipate to observe a temperature rise. While this is indeed the case, the magnitude of the rise, however, is typically small, thus negligible. For this reason, the coupled thermoelasticity is often simplified to the *theory of thermal stress* [27], by ignoring the last term in (1.50), which is a heat generation effect related to the rate of solid deformation. The dropping of the heat generation term makes the theory of thermal stress *uncoupled*; that is, (1.50) can be solved independent of (1.49). This is certainly not the case for poroelasticity.

The above analogy can be further compared through the following experimental setup. Suppose that we test a thermoelastic and a poroelastic body for their bulk moduli based on formula provided in Sect. 1.2.1. For the thermoelastic body, we can conduct the test under the *adiabatic* condition, that is, by insulating the sample from heat flow, or under the *isothermal* condition, that is, by maintaining constant temperature throughout the test. Experience tells us that the two material constants measured, an *adiabatic bulk modulus* and an *isothermal bulk modulus*, are basically indistinguishable. For poroelasticity, we can identify the adiabatic condition with the undrained condition, and the isothermal with the drained, based on the above-mentioned analogy. Following the discussion in Sect. 1.2.1, we know that the drained and undrained bulk moduli are drastically different; hence the uncoupling of the thermoelasticity theory may be proper for most applications, the uncoupling of poroelasticity, on the other hand, should not be attempted.

As discussed above, the heating of an elastic body generates a thermal stress, and equivalently, the flooding (injection of fluid mass) of a poroelastic body generates a *poroelastic stress*. Similar to the concept of a material constant known as thermoelastic stress coefficient, we can define its counterpart as a *poroelastic stress coefficient*. Under certain conditions, there exists a simple relation between the pressure increment and the generated poroelastic stress. This condition exists in an unbounded (large) domain that is initially under a constant confining stress and pore pressure. When a portion of the domain is flooded by fluid injection to

create a distribution of pore pressure increment p, the corresponding generation of poroelastic confining stress is given by [42]

$$-\frac{\sigma_{xx}+\sigma_{yy}+\sigma_{zz}}{3}=\frac{4}{3}\eta p \tag{1.55}$$

in which η is a poroelastic stress coefficient, given by

$$\eta=\frac{\alpha(1-2\nu)}{2(1-\nu)} \tag{1.56}$$

where ν is the *Poisson ratio*. The coefficient has the value $0 \leq \eta \leq 0.5\alpha \leq 0.5$.

Or, in the case of a *plane strain* condition, that is, the body is confined from movement in one of the directions, $u_z = 0$, the poroelastic stress generated becomes

$$-\frac{\sigma_{xx}+\sigma_{yy}}{2}=\eta p \tag{1.57}$$

And if the displacement is allowed only in one direction, elected as x, we observe

$$-\sigma_{xx}=2\eta p \tag{1.58}$$

Typical values of η are given in Table 3.2.

1.2.8 Coupled Versus Uncoupled Diffusion

As mentioned in Sect. 1.2.2, Terzaghi's original consolidation theory [234] was characterized by a one-dimensional diffusion equation given as (1.13). To deal with multi-dimensional consolidation problems, the theory has been generalized in an ad hoc fashion to a three-dimensional form by Rendulic [200] and Terzaghi [237], as the following

$$\frac{\partial p}{\partial t}-c\nabla^2 p=0 \tag{1.59}$$

The Biot theory [16], however, shows that the simple diffusion equation is satisfied not by p, but by ζ, the relative volumetric strain between the porous medium frame and the fluid, as given by (1.53). Based on its definition, ζ is dependent not only on the pore pressure, p, but also on the volumetric strain, e. Converting (1.53) to these variables, we obtain (1.48), which shows that the pressure diffusion is coupled with the solid deformation, and cannot be independently solved. The right hand side of (1.48) shows that the rate of change of volumetric strain serves as a source term for pore pressure; that is, as the pore pressure is being dissipated, the solid continuously deforms (due to the change in effective stress), and new pore pressure

is continuously generated. Or, another way to view the pore pressure diffusion equation is to express it in the following form

$$\frac{\partial p}{\partial t} - \frac{\kappa KM}{K_u}\nabla^2 p = -\frac{\alpha M}{3K_u}\frac{\partial \sigma_{kk}}{\partial t} \tag{1.60}$$

where $\sigma_{kk} = \sigma_{xx} + \sigma_{yy} + \sigma_{zz}$. The above equation shows that the rate of change of compressive stress also serves as a pore pressure production term.

In conclusion, the poroelasticity theory shows that pore pressure diffusion is a process coupled with the solid deformation, and the Terzaghi-Rendulic three-dimensional uncoupled diffusion equation (1.59) is missing an important physical mechanism, hence is incorrect. We should however mention that Terzaghi's one-dimensional consolidation equation (1.13), as a special case, is in fact consistent with (1.48) and (1.60), if the soil stratum is restricted to deform only in the vertical direction, and the surcharge on top of soil remains constant with time.

1.3 Poroelastic Phenomena

With the basic understanding of the physical mechanisms underlying the poroelastic effects, we are ready to examine a few observed poroelastic phenomena and to explore their physical interpretations.

1.3.1 Borehole Failure

In deep geological formations, rock is subjected to a large compressive stress, which is either caused by the weight of rock mass above it, or by tectonic movement. If a circular hole is drilled through the formation, and left empty, elasticity solution predicts a maximum stress located on the borehole wall in the circumferential direction, which is twice that of the in situ stress. If this maximum compressive stress exceeds the ultimate compressive strength of the rock, it will fail instantly. The collapse of a borehole, however, is sometimes found to be time-delayed; that is, not happening at the time of the drilling, but at some later time [83, 183, 196]. Elasticity theory cannot explain such phenomenon. For shale, which is characterized by extremely low permeability and high chemical activity, this delay can be days to weeks. While this delay can be attributed to a number of factors, such viscoelastic creep and chemical reaction of shale, poroelastic effects certainly play an important role. We shall examine one such scenario of delayed borehole failure below.

Assume that a circular borehole is instantly drilled in an infinite domain initially under a uniform stress, $\sigma_{xx} = \sigma_{yy} = -P_o$, and constant pore pressure $p = p_o$ (Fig. 1.3). At the borehole wall, $r = a$, such conditions need to be satisfied: $\sigma_{rr} = 0$ and $p = 0$. For the elastic response, the described problem is just the classical Lamé problem [147], whose solution in terms of stresses is given by [129, 246]:

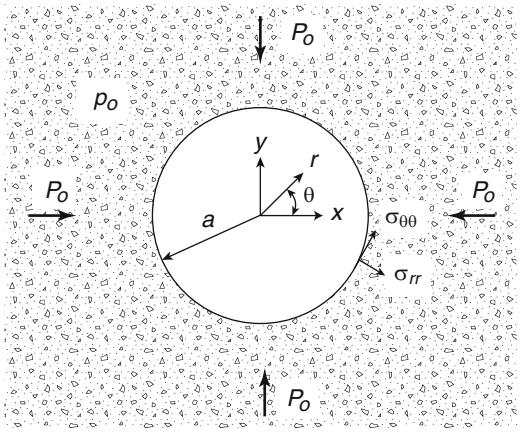

Fig. 1.3 Borehole in an uniform stress field

$$\sigma_{rr} = -P_o\left(1 - \frac{a^2}{r^2}\right) \tag{1.61}$$

$$\sigma_{\theta\theta} = -P_o\left(1 + \frac{a^2}{r^2}\right) \tag{1.62}$$

where σ_{rr} and $\sigma_{\theta\theta}$ are the normal stresses in the radial (r) and circumferential (θ) directions, respectively. We can easily observe from the above solution that as $r \to \infty$, $\sigma_{rr} = \sigma_{\theta\theta} = -P_o$, and as $r \to a$, $\sigma_{rr} = 0$, fulfilling the stated boundary conditions. Of interest to observe is that at the borehole wall a stress concentration is developed in the circumferential direction,

$$-\sigma_{\theta\theta}|_{r=a} = 2P_o \tag{1.63}$$

which is twice the magnitude of the original compressive stress.

As discussed in Sect. 1.2.1, the poroelastic body at the instant of loading is undrained, and behaves as an elastic body. Hence the above solution, (1.61) and (1.62), is indeed the stress state for a poroelastic body at $t = 0^+$. In Sect. 1.2.3, we also showed that at that instant, there is a pore pressure rise proportional to the increment of average compressive stress, given by (1.19) for plane strain condition. There is, however, a curiosity about the present solution, (1.61) and (1.62). It is easily shown that

$$-\frac{\sigma_{rr} + \sigma_{\theta\theta}}{2} = -\frac{\sigma_{xx} + \sigma_{yy}}{2} = P_o \tag{1.64}$$

So there is no change in the *average* compressive stress everywhere in the formation, before and after the excavation of the borehole. This means that there is no new pore pressure generated, and it stays everywhere as p_o. With these results, we are ready

to conclude that at the instant of the excavation, there is a Terzaghi effective hoop stress of the magnitude

$$-\sigma'_{\theta\theta}\big|_{r=a,t=0+} = 2P_o - p_o \tag{1.65}$$

developed around the borehole wall, which is increased from the original formation effective stress of $P_o - p_o$.

Next, we consider the stress condition around the borehole at large time. As time progresses, two mechanisms are taking place. One is more obvious: the pore pressure at and near the wall is dissipated, $p \to 0$; hence the protection provided by pore pressure against effective compression no longer exists. A less obvious mechanism can be explained using the thermoelastic analogy discussed in Sect. 1.2.7. The dissipation of pore pressure is equivalent to the cooling of solid around a hole. As the temperature at larger distance remains high, a tensile stress develops around the hole. In the poroelastic case, a relief of the compressive stress in the amount ηp_o results (see (1.57)). Hence the final effective hoop stress at the borehole is

$$-\sigma'_{\theta\theta}\big|_{r=a,t\to\infty} = 2P_o - \eta p_o \tag{1.66}$$

Comparing (1.65) with (1.66), we observe an increase of effective compressive stress near borehole wall of the magnitude $(1 - \eta)p_o$, which can be a cause for the delayed failure [42, 70].

In a drilling operation, to prevent the borehole from collapsing, the hole is filled with a drilling mud. The hydrostatic pressure of the mud pushes back the formation to provide support on the wall. However, when the mud weight becomes too large, it can more than compensate the inward compression, and push the borehole wall into tension. If the tension exceeds the tensile strength of the rock, fracture can initiate at the wall, and propagate into the formation. This is generally an unwanted result.

However, there are occasions that fractures are intentionally created in an operation called *hydraulic fracturing* [116]. In such application, an uncased section of the borehole is sealed off at top and bottom using packers. Fluid is injected into this interval to raise the pressure to initiate a fracture, and then continuously to drive it into the formation. The artificially created large fracture can be used to increase the hydraulic conductivity of reservoir to stimulate the hydrocarbon production. In such operations, it is of interest to predict the *borehole breakdown pressure*, p_b, that is, the minimum borehole pressure that can initiates a fracture.

As early as 1953, Scott et al. [214] observed in a laboratory setting simulating hydraulic fracturing that thick-walled hollow cylindrical cores could be ruptured using penetrating fluids at less than half the pressures required as compared to using non-penetrating fluids. As the difference between these two cases is fluid penetration into the rock specimen, it is apparent that poroelastic effects are at play.

Based on only elasticity consideration, the breakdown pressure for a borehole in a non-hydrostatic (anisotropic) stress field can be predicted by

$$p_b = 2P_o - 4S_o + T \tag{1.67}$$

where P_o and S_o are respectively the far-field mean stress and stress deviator, and T is the tensile strength of the rock. To take into consideration the effective stress in the presence of pore pressure, Hubbert in 1957 [122] modified the above formula, assuming non-penetration fluid and that the pressure at the borehole wall is that of the formation pore pressure p_o, to the following

$$p_b = 2P_o - 4S_o + T - p_o \tag{1.68}$$

As the pore pressure at the wall is generally not that of the virgin pore pressure, Detournay and Cheng [70] presented the upper bound of breakdown pressure as

$$p_{bu} = 2P_o - 4S_o + T - 2\eta p_o - (1 - 2\eta)p_i \tag{1.69}$$

where p_i is the pore pressure at the borehole wall, $p_o > p_i > 0$, and the coefficient η arises from the poroelastic stress effect, as explained in Sect. 1.2.7. Haimson and Fairhurst [106, 107] considered the penetrating fluid case to give

$$p_{bl} = \frac{2P_o - 4S_o + T - 2\eta p_o}{2(1 - \eta)} \tag{1.70}$$

where p_{bl} stands for the lower bound of breakdown pressure. Depending on the mud used for fracturing, the true breakdown pressure should be between these two limits, p_{bl} and p_{bu}.

Small scale hydraulic fracturing can be used as a way to measure the in situ stress of a formation [82, 139]. In such practices, pressure is continuously raised in a section of the borehole, until a sudden drop-off of pressure is observed, reflecting a situation where the rate of fluid loss, due to fracture extension and fluid leakoff, becomes greater than the pumping rate. Further injection of fluid causes the fracture to propagate, and reorient in the direction perpendicular to the minimum in situ stress. After pumping is stopped and the well is *shut in*, the pressure in the sealed-off interval decays because of further fracture propagation and fluid leakoff into the formation. At some stage, the newly-created fracture will close. Interpretation of in situ stress from hydraulic fracturing tests relies on the *fracture closure pressure* measured during shut-in, and also on the *breakdown pressure*, measured during the first pressurization cycle, or the *reopening pressure*, measured during subsequent pressurization cycles [105, 108, 112]. Poroelastic effects in the determination of in situ stress using the above information have been investigated [72, 73].

In the above we discussed borehole failure when the stress level exceeds its compressive or tensile strength. Borehole can also fail by shear, when the ratio of shear to normal stress exceeds the shear strength of the material, based on the *Mohr-Coulomb* failure theory. This is often observed as borehole *breakout* in deep wells; that is, the spalling of rock on two symmetric sides of the wall, making the hole into an elongated shape. Elasticity solution indicates that in the presence of an anisotropic stress field, breakouts are aligned in the minimum principal in situ stress direction; hence breakout observation has been used as a way to determine the in situ

stress directions [100, 189, 276, 278]. Elasticity solution also predicts an initiation of shear failure right at the borehole wall. Poroelasticity solution, however, shows that the shear failure initiation can take place at a small distance, about 5–10 % the borehole radius, inside the borehole wall [42, 70], which may explain the finite size rock debris, and the progressive failure in time, found during breakout events.

1.3.2 Mandel-Cryer Effect

To demonstrate the coupled effect of pore pressure diffusion and solid deformation in the poroelasticity theory, in contrast to the uncoupled diffusion in the Terzaghi-Rendulic three-dimensional consolidation theory (see Sect. 1.2.8), Mandel in 1953 [160] and Cryer in 1963 [55] each presented analytical solution that exhibits the curious response of non-monotonic pore pressure diffusion, characterizing the coupled theory. Such phenomenon of pore pressure continues to rise after its initial generation, before it declines to zero due to diffusion, has been called the Mandel-Cryer effect [211].

The Mandel problem is illustrated in Fig. 1.4a, which shows a poroelastic specimen sandwiched between two rigid, impermeable platens with frictionless surfaces. A force F is suddenly applied to these rigid platens, resulting in a uniform pore pressure rise p_o throughout the specimen, based on the Skempton effect. Because the sides of the specimen are exposed to atmosphere, this pressure will drive a horizontal seepage flow toward the drainage surfaces, and dissipates to zero with time. If the pore pressure obeys the uncoupled diffusion equation (1.59), the decline will be monotonic, from p_o to zero. The Mandel solution, however, shows that the pore pressure will first rise above the initially generated value, before it falls. This phenomenon can be explained as follows.

As the porous specimen is homogeneous, at the instant of the applied force, the load is uniformly distributed, giving a constant vertical compressive stress $-\sigma_{zz}$

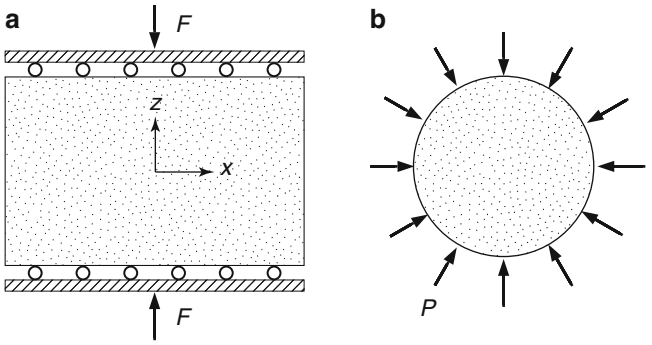

Fig. 1.4 (**a**) Mandel problem, and (**b**) Cryer problem

throughout the specimen. As the pore pressure starts to dissipate near the left and right edges, the material effectively softens as the fluid is taking less load. Effectively, the material becomes inhomogeneous with a harder core and softer edges. This will cause the load to redistribute, resulting in a higher $-\sigma_{zz}$ near the center. Eventually, the entire pore pressure will dissipate, and σ_{zz} will return to uniform again.

As demonstrated in (1.60), the rate of increase of compressive stress is a pore pressure generation mechanism. Hence at any point inside the specimen, the pore pressure is experiencing two opposing trends, a diffusion process making it to monotonically decline, and a pore pressure generation making it to rise. As the diffusion process takes time, at any point inside the specimen, it will first experience an elastic load transfer due to the diffusion taking place nearer to the edges, before the arrival of the diffusion front to dissipate the pressure. Hence we observe a non-monotonic behavior.

The Cryer problem is similar to the Mandel problem, but with a different geometry. Cryer solved the problem of a saturated spherical soil specimen suddenly compressed by an inwardly pointing uniform radial stress on its surface (see Fig. 1.4b). At $t = 0^+$, a uniform compressive stress and pore pressure develop everywhere inside the specimen. At the surface of the sphere, water can escape freely, so the specimen will consolidate in time. Cryer's analysis showed that during the early stages of consolidation the pore water pressure at the center of the sphere could rise almost 60 % above the initial pressure, before it starts to decline.

The physical explanation for the non-monotonic response is similar to that of the Mandel problem. As the pore pressure near the surface starts to dissipate, effectively the sphere becomes an inhomogeneous material with a softer outer shell and a stiffer inner core. This will result in an increase of total compressive stress in the inner part of the sphere. (Or, consider the opposite: a harder outer shell can protect an inner softer core, subjecting it to a lower stress.) This increase of compressive stress again serves as a pore pressure generation mechanism, giving the non-monotonic pressure behavior. This phenomenon predicted by the Cryer solution [55] was soon demonstrated in the laboratory [99, 255].

1.3.3 Noordbergum Effect

Verruijt in 1969 [256] reported a phenomenon in the well field of the small village of Noordbergum, in the Netherlands. When pumps were turned on to extract water from the upper, confined aquifer of a two-layer leaky aquifer system, it was anticipated that the water level (piezometric head) will drop in both the pumped upper aquifer and the unpumped lower aquifer, based on the leaky aquifer theory [110]. It was however curiously observed that at a distance from the pumping wells, water level in monitoring wells located in the lower aquifer actually rose for a period of time, before dropping. Verruijt [256] provided an approximate analytical solution based on poroelasticity theory, and demonstrated such reversal effect, which has

been called the *Noordbergum effect* [205]. Verruijt explained such phenomenon by referring to poroelastic effects as follows: "*Due to the decreasing pore water pressures in the upper layer; this layer will attract water from the upper part of the lower layer. The loss of water involves a decrease in volume of the upper part of the lower layer. All elements of a circular ring around the origin will decrease in volume, thus producing a radial displacement towards the center to keep the ring closed. For the lower parts of the layer, this radial displacement presents a loading due to which a tendency for compression will be present. Since the pore water opposes volume compression of the soil, this results in an increase of the pore water pressure*." Verruijt compared the solution with pumping tests conducted at the polder Vierbannen, on the island of Schouwen-Duiveland, the Netherlands [253], and obtained good agreement.

Wolff [262] pointed out that the "abnormal" water level responses after pumping activities had been observed in many occasions since 1936 [9]. These phenomena were generally referred to as *reverse groundwater level fluctuations*. Langguth and Treskatis [148] reported a similar phenomenon observed in the well field of Rhade Lowland near Dorsten, in southern Münster basin, Germany. In a well installed with a multilevel piezometer to monitor piezometric head in the aquifer as well as the overlain aquitard, when pumping started in the aquifer, the Noordbergum effect was observed in the aquitard. When the pump is shut off, the piezometric head in the aquitard dropped, rather rapidly, for a short while, before it recovered to the original level before pumping. Hence we may refer the decline in head in the adjacent aquifer or aquitard at the beginning of groundwater pumping the *Noordbergum effect*, and the drop in head after the end of pumping the *Rhade effect*. Based on numerical solutions, Kim and Parizek [141, 142] were able to simulated both effects using poroelasticity theory.

The above discussion involves the observation of reverse water level in aquifers and aquitards adjacent to the pumped aquifer. In fact, this type of behavior can exist in the pumped aquifer as well. The Theis solution of groundwater flow [13, 41] predicts that as pumping starts in a confined aquifer, the head in the aquifer declines everywhere. Numerical simulation based on poroelasticity, however, shows that at a distance from the well, the head rises first, before it falls [104, 272].

In Fig. 1.5 we provide a simple illustration of such a physical process, but in reversal—that is, rather than extracting from the aquifer, water is injected into it. The aquifer is assumed to be confined from above and below by impermeable layers. The overburden layer on top is assumed to have a certain degree of flexural rigidity, that is, a non-zero shear strength. As the formation is being flooded by the injected water, there is a cylindrical region surrounding the well with significant head rise such that the overburden formation is pushed up, like a subsidence in reverse. With a finite flexural rigidity, the formation arches up like a dome. In the region ahead of the significant pressure rise, the pressure first drops due to the uplift of the overburden layer, until the pressure front eventually reaches the region.

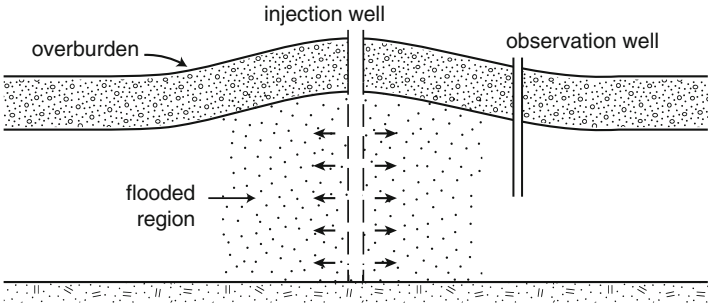

Fig. 1.5 Noordbergum-like effect due to uplift of overlain formation

1.3.4 Land Subsidence

Land subsidence is the settling of ground surface over large areas, due to the compaction of subsurface materials, primarily clay layers or lenses, usually as a consequence of pumping from underlying aquifers. It can also be the result of producing oil and gas from underground hydrocarbon reservoirs. The term *consolidation* is used for the similar land settlement phenomenon, when it occurs over relatively small areas, especially as a result of loading ground surface, e.g., by new structures.

The turn of the twentieth century witnessed an explosion in oil production and large scale irrigated agriculture. These activities very soon led to noticeable environmental effects including land subsidence. The first observed land subsidence due to subsurface fluid withdrawal was reported by Pratt and Johnson in 1926 [192] from the Goose Creek oil field, near Galveston, Texas. The first recorded land subsidence due to groundwater withdrawal was fortuitously discovered around San Jose, California in 1932, by the U.S. Coast and Geodetic Survey, during repeat precision-leveling [174, 198].

There exist many examples of subsidence over large areas as a result of pumping groundwater [190]. Perhaps, the most spectacular one in an urban area is in Mexico City, where almost the entire metropolitan area has subsided more than 3 m (with up to 8 m at some locations). As a result of excessive withdrawal of groundwater for irrigation, the San Joaquin Valley in California has experienced subsidence at a rapid rate of 30–40 cm per year, reaching a total subsidence of 9 m at some locations. Another well-known case is Venice, Italy, where all pumping has ceased in an effort to stop further land subsidence. Many measures have been suggested to prevent Venice from "sinking". One method suggests pumping seawater into deep aquifers to uplift the land surface [95, 232].

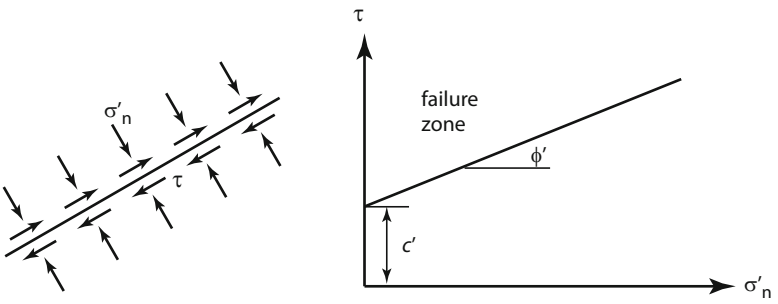

Fig. 1.6 Mohr-Coulomb shear failure criterion

1.3.5 Slope Stability and Fault Slippage

Mohr-Coulomb theory is a widely accepted criterion of shear failure for brittle and granular materials, or materials for which the compressive strength far exceeds the tensile strength. Most porous materials fall into this category. The criterion is a linear relation between the shear stress τ and compressive normal stress σ_n (for convenience, compression is considered positive in this section only), given as

$$\tau = c' + \sigma_n \tan \phi' \tag{1.71}$$

where c' is an internal strength of the material, known as *cohesion*, and ϕ' is the *angle of internal friction*. The above equation defines a *failure envelope* on the σ_n-τ plane (see Fig. 1.6). When a pair of normal and shear stress falls above the envelope, the shear stress is then too large for the strength of the material to sustain, and the material will fail.

Terzaghi [238] has modified the above equation by replacing the normal stress with the effective normal stress, to become the following

$$\tau = c' + (\sigma_n - p) \tan \phi' \tag{1.72}$$

which has been successfully used to predict the slope stability of soil embankment. Although there exists the more sophisticated *critical state* soil failure theory [212, 213], for the present purpose, we shall use the Mohr-Coulomb theory to explain the role of pore pressure in the failure of porous materials.

It is well known in soil mechanics that soil saturation and the rise of water table tend to destabilize embankment, increasing the risk of landslide. When water table rises, it has two effects: first, it adds to the overburden weight on the underlying soil, increasing its normal stress; and second, it develops a hydrostatic pore water pressure, which reduces the effective normal stress according to (1.72). The normal stress added by the weight of water is proportional to the water density, the elevation of the water table, and the porosity. The reduction of normal stress, however, is

dependent only on the water density and elevation of water table, and independent of porosity. Effectively, there is a reduction of normal stress that is equivalent to subjecting the solid to a buoyancy force by water. As the shear stress is unaffected by the water saturation, the reduction in normal stress tends to shift the stress state on the σ_n-τ plane to the left, such that it may cross the failure envelope, leading to sliding failure.

In a partially saturated (capillary) zone, the pore pressure is negative, due to the surface tension of water meniscus. Based on the effective stress concept, there is an increase in the effective normal stress, which tends to stabilize the soil. This is how one can build sand castle using wet (partially saturated) sand, and not dry sand. On the other hand, if the castle is submerged in water and become saturated, it collapses.

Similar stability issue exists for fractures or faults found in geological formations. Pre-existing fractures and faults are discontinuity surfaces that have little or no tensile strength perpendicular to the surface. Its strength against sliding is dependent on the material strength as well as the roughness of the discontinuity surface. A normal force can reduce the potential of sliding, with a stability criterion similar to that of Mohr-Coulomb law. Increasing pore pressure around a fault causes reduction in effective normal stress and can induce fault movement.

In 1959 Hubbert and Rubey [121, 209] introduced such concept to explain the puzzling paradox of the *overthrust faulting* found in Earth's crust. In a thrust fault, a large block of rock sheet is thrust to slide against another rock sheet, and is moved over a great distance. In these provocative papers written at that time, Hubbert and Rubey calculated the force needed to thrust one rock sheet to overcome the friction between the two sheets and to slide, and concluded that the force would far exceed the crushing strength of the rock in the typical overthrust faults found in Canadian Rockies and Appalachians. They then hypothesized the role of fluid pressure in the effective stress concept. They argued that if fluid pressures within the faulting plane became sufficiently high, the effective friction strength could dramatically decrease, enabling the transport of enormous rock blocks over long distances with smaller thrusting force.

To allow people to visualize the effect, Hubbert and Rubey [121] experimented on the "beer can experiment", originally suggested by M. A. Biot. In such experiment, an emptied beer can is placed upside down over a clean glass plate wetted with water. The plate is raised to a certain angle to allow the can to slide down the plane due to gravity pull. Hubbert and Rubey reported that the inclination angle needed was about 17° (for the heavier beer can in those days). The beer can is then chilled in a freezer, taken out, and the experiment is repeated. A small amount of time is allowed for the air entrapped in the can to warm and for the air pressure to increase. The beer can is then able to slide down the plane at less than 1° inclination. The reason is that the air pressure produces an uplift force that offsets the normal stress exerted on the glass plate. Nowadays the concept of pore pressure and effective stress is well received in structural geology [60].

1.3.6 Fluid Induced Seismicity

An geological event that is of man-made origin is the fluid induced seismicity [220]. It has been reported that during the injection of liquid nuclear waste into deep formation at a site near Denver, Colorado, an M5.5 earthquake was generated [113, 118]. Similarly, water injection at Cogdell Canyon Reef, Texas, for the purpose of secondary oil recovery, induced a M4.6 earthquake [62]. In the hot dry rock geothermal project at Fenton Hill, New Mexico, hydraulic fracturing is used to create flow path to enhance water circulation. During the hydraulic fracturing process, hundreds of micro earthquakes were detected [184, 187].

In yet another man-made situation, the impoundment of reservoirs can induce seismic events, which was reported as early as 1945 by Carder [36], and many more evidences were collected by Simpson [225]. The underground stress environment is changed not only by the weight of impounded water, but also by the invading pore pressure induced by seepage, which can alter the effective normal stress of pre-existing fracture. A number of reservoir impoundment induced earthquakes exceeding M6 have been recorded all around the world [102]. The 1967 Koyna, India earthquake of M6.3 is so far the largest and most damaging reservoir triggered earthquake [103]. A poroelastic modeling of the fault stability due to cyclic water level fluctuation has been conducted [206].

The pore pressure effect can manifest itself in many different ways. Not only the injection of fluid into formation, but also the extraction of fluid from it, can induce seismic events. As discussed in Sect. 1.2.7, the flooding of a smaller region contained within a larger (infinite) domain with a uniform pressure p induces an apparent increase of far-field confining stress of the magnitude $4\eta p/3$. At the same time, within the flooded region, the pore pressure also causes a reduction in compressive effective stress of the magnitude p. Hence the net effect is to destabilize a fracture within the flooded region. Extracting fluid has the opposite effect. Within the region of pressure decline, it experiences a reduction of far-field confining stress. This reduction, however, can extend a few distances beyond the size of the fluid decline region, with diminishing magnitude, as controlled by the elastic behavior. Outside the pressure decline region, there is no pore pressure to change the effective stress, hence the reduction in normal stress can destabilize a fracture outside the extraction region and cause it to slip. Fluid extraction induced earthquakes in fact have been observed [185, 216, 268], and modeled as a poroelastic effect [217, 229].

In the above we have discussed events triggered by man-made actions perturbing the underground environment. Pore pressure can also play an important role in many naturally occurring geophysical events, such as earthquakes [52, 91]. Nur and Booker [28, 178] were among the first to suggest that the time delayed *aftershock* events following a major earthquake can be explained by the poroelastic effects. Large shallow earthquakes alter the stress in the surrounding crust. While some parts of the earth may be relaxed, other parts are compressed. This stress redistribution can induce changes in the fluid pore pressure with magnitude that are comparable to stress drops on faults. The subsequent fluid flow and pore pressure redistribution can

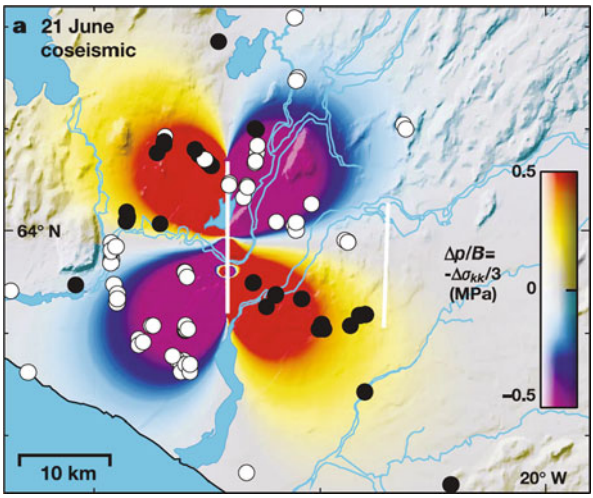

Fig. 1.7 Coseismic water level changes in geothermal wells in South Iceland. Water level increase is shown in black dots and decrease in white dots (From Jónsson et al. [136], with permission)

cause the pressure to decrease in the compressed region, and increase in the dilated region. Many smaller faults and fractures that are momentarily at rest after the major event can be at the critical state against sliding. The invasion of pore pressure can reduce the effective normal stress locally and trigger the aftershock events [218].

Other poroelasticity effects include the earthquake precursory effects due to pore fluid stabilization of a weakening fault zone [202], and the pore water diffusion to the dilating tip of the shear rupture zone (*shear band*) to stabilize it against rapid propagation in over-consolidated clay [181].

In Fig. 1.7 we present an interesting seismic observation. The South Iceland seismic zone is a left-lateral transform zone, where east-west transform motion is accommodated by north-south-oriented right-lateral faults. The earthquakes on June 17 and 21, 2000, ruptured two of these faults. During the earthquake period, water level changes were observed in numerous geothermal wells. The sign of the water level changes exhibits a quadrant pattern, as shown in Fig. 1.7 [136]. In Chap. 8 we shall derive the poroelastic solution of a *slip point dislocation*. A point dislocation is a *displacement discontinuity* at a point where the formation breaks apart and moves in opposite directions. The motion can be in an opening mode or a slipping mode. In Fig. 1.8 we plot the contour lines of pore pressure response created by the slipping motion. We can see the resemblance of the pattern of pore pressure field as compared to the field observed water level after the slippage of fault, shown in Fig. 1.7.

1.3.7 Outburst of Coal

Underground coal gasification is an in situ gasification process carried out in low grade coal seams that are not economical to mine, and the coal is burned underground without sufficient oxygen to produce methane gas. Injection wells are

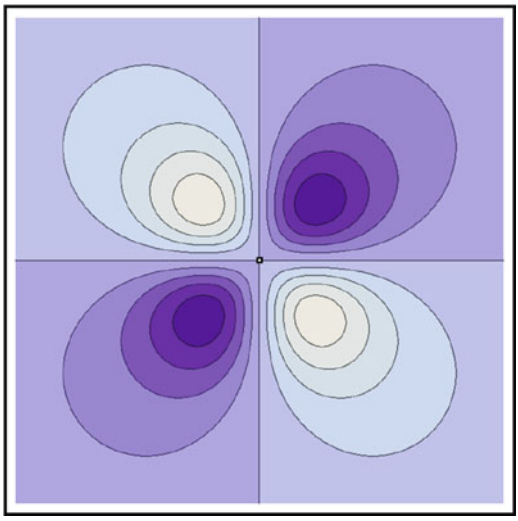

Fig. 1.8 Contour plot of pore pressure generated by a slipping displacement discontinuity

used to supply the oxidants (air, oxygen, or steam) to ignite and fuel the underground combustion process. Separate production wells are used to extract the product gas to surface.

In order to create an initial surface large enough to start the burning process, either hydraulic fracturing or the *cavitation* technique has been be employed [153, 163]. For the cavitation technique, in a process called *open-hole completion*, air is injected into coal seams through an uncased wellbore interval with high pressure. The pressure is sustained for a period of time to allow it to permeate into the formation, and then suddenly released. The sudden drop in pressure induces tensile failure of the coal in various orientations around the wellbore. As the weak, friable coal sloughs in, the wellbore is enlarged. (See Sect. 7.15.2 for a theoretical exposition.) This process can be repeated several times. In fact, this process can be a byproduct during production in a *dynamic open-hole completion* technique, in which air or an air-water mixture is repeatedly injected into an open-hole interval, followed by immediate release of wellbore pressure, and the cavity is continuously being enlarged during production.

This cavitation phenomenon can be attributed to the poroelastic effects. When the wellbore is pressurized for a period of time, a high gas pressure region is built up surrounding the borehole. Just before venting, the hole is stable as there is a radial stress pushing against the wall. However, when the air in the hole is instantly vented, the radial compressive stress on the wall is reduced to zero. Inside the formation, due to the presence of an overpressure, the effective radial stress becomes in tensile range. Since the tensile strength of coal is very small, the wall collapses by tension. This phenomenon has been simulated as a consequence of the poroelastic mechanism [37, 38, 42].

In fact, in coal mine operation, it is well known that when excavation reaches regions over-pressurized by methane gas, and the surface is exposed and

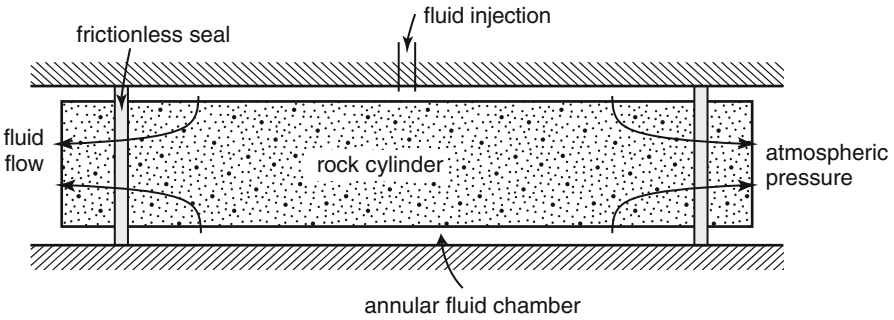

Fig. 1.9 Pinch-off test to break a rock cylinder by tension

unsupported, an explosive type of failure can take place, known as *outburst* [12]. Hence it is important to drill pilot holes ahead of mining excavation to vent methane gas, for the purpose of preventing not only the ignition of the combustible gas, but also outburst and cave-in. The poroelastic interpretation of this phenomenon has been investigated [182, 275].

The above described phenomenon may sound curious—there is no external physical force pulling the coal, yet it breaks off by tension! Is it possible? In fact, this effect can be demonstrated in laboratories using the so called "pinch-off" test of Bridgman [32], and modified by Jaeger and Cook [128]. Cylindrical rock core can be placed in a fluid chamber as illustrated in Fig. 1.9. Radial seals are positioned near the ends to confine the fluid in the chamber. Seal lubricant is applied to minimize the friction resistance in the cylinder axial direction [128]. Water is injected into the annular chamber between the core and vessel. The ends of the core are open to atmosphere so that there is no axial stress applied to the core, and fluid is allowed to flow out at the ends by permeation [34]. Fluid pressure in the chamber is slowly increased until the core ruptures by tension. The breakage takes place when the fluid pressure is of the order of, and slightly larger than, the tensile strength of the rock core [128]. A simple explanation is that although the axial stress σ_{zz} is zero, the Terzaghi effective axial stress σ'_{zz} is in tension with the magnitude of the pore pressure [127].

1.3.8 Hydraulic Fracturing

Hydraulic fracturing, a well stimulation technique first suggested by Clark in 1949 [47], has been widely used in oil and gas industry for enhancing underground hydrocarbon recovery. The mechanics of hydraulic fracturing was first rigorously examined by Hubbert in 1957 in his classic paper [122]. Later development in the theory and technology is well covered in a few comprehensive books [79, 116, 250, 269].

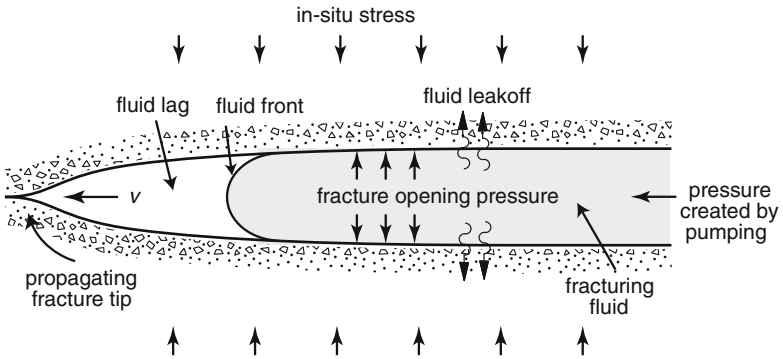

Fig. 1.10 A horizontal cross-section of a vertical hydraulic fracture

The concept of hydraulic fracturing is to greatly increase the production surface area of porous medium, where oil or gas can be collected, from that of a borehole wall to a massive fracture driven into the formation. The fracture is created by pumping at high pressure a fracturing fluid into a section of the wellbore to first break the formation by tension, and then continuously driving a contained fracture, typically vertical in orientation, into the *pay zone* (hydrocarbon containing formation). Containment of the fracture is important because penetration into the adjacent formations may mean producing a mixture of water and oil that is difficult to separate, or contaminating the water bearing aquifers. With careful design and field control, fractures can reach several hundred feet in distance.

To drive a fracture, a significant amount of pumping pressure is needed to overcome not only the formation in situ stress pushing to close the fracture, but also the large flow resistance caused by a number of factors, including the narrowness of the aperture, the roughness of the fracture surface, and the high viscosity of the fracturing fluid (see Fig. 1.10). Using a model combining solid fracture mechanic and non-Newtonian fluid flow in the aperture, it is possible to predict the pumping pressure required to create a designed fracture. It was found that these models generally underestimate the pumping pressure needed to create a given fracture, even if the fluid loss into the formation was taken into consideration [175, 228].

One mechanism proposed to account for the extra pumping pressure needed is the poroelastic stress effect, otherwise known as the *backstress* in hydraulic fracturing terminology [50, 51, 73]. As the fluid pressure in the fracture is higher than the formation pressure, a loss of fracturing fluid through infiltration into the formation will take place, known as *leakoff*. With a rise of pore pressure, the flooded region will expand, as explained by the thermoelasticity analogy in Sect. 1.2.7. This expansion tends to close the fracture, as if there exists an extra confining stress at the far-field; hence it is called a “backstress”.

Other poroelastic effects considered include the gradual opening of a stationary hydraulic fracture due to the large time, drained response of the formation in the far-field, making the material effectively more compliant. This is then offset by

the backstress effect due to the fluid penetration in the near-field, resulting in a combined large time fracture response of gradual decrease in fracture width [71].

The small and large time (undrained and drained) response of poroelastic medium also causes a time dependent stress concentration on the fracture tip [71]. Based on the same concept, the speed of a propagating fracture tends to have a stabilization effect, as the higher the speed, the more undrained (stiffer) the material behaves, hence resisting the propagation at an even higher speed [44, 203, 224]. If the stress intensity factor falls between the drained and undrained limits, a stable, constant speed propagating fracture can be maintained.

In another utilization of poroelastic effects, it is possible to attract a propagating fracture toward a target well by creating a favorable propagation path. In many applications, it is highly desirable to connect two wells with a fracture. Under normal condition, it is nearly impossible to control the fracture path other than utilizing the in situ minimum principal stress direction. With poroelastic effect, it is possible to pressurize a target well ahead of time to flood the region surrounding it, in order to reduce the effective compressive stress, and to attract the fracture initiated at another well toward the target well [15].

In present day, hydraulic fracture is used not only in oil and gas industry, but also in a number of other applications, such as injecting liquid nuclear waste into geological formations for isolation and disposal [67, 68], using water [77, 90, 149] or CO_2 [33] as injection fluid to create fracture to circulate water in enhanced geothermal systems (hot dry rock), creating horizontal fracture as a means of enhancing pump-and-treat, soil vapor extraction, and in situ environmental remediation in shallow soil, for pollutants such as heavy metals and hydrocarbon waste or spills [89, 173, 221], and stimulating groundwater production by connecting naturally occurring fractures in rock formations [247].

The hydraulic fracturing discussed above refers to the technology that creates a single, or a few, large fractures initiated mostly from a vertical well, and occasional from a horizontal well. With the advancement of the technology of directional drilling, and the need for new energy resources, a new technique, popularly known as *fracking*, has become wide spread in the oil and gas industry in the last decade. A vertically drilled well can only intersect a small length of a horizontal pay formation. Directional drilling allows a well to trace the formation in the horizontal direction to create a large length of wellbore section for hydrocarbon collection. The hydraulic fracturing technique now takes a different aim—instead of creating a single, large fracture from a vertical well, it aims at the creation of a large number of shorter, closely spaced, and interconnecting fractures from a horizontal well. The technique allows the production from the *unconventional reservoir* such as shale gas formation, also known as *tight gas reservoir*. "Tight" means very low permeability such that production using conventional technique is not economically feasible. This fracking technology opens the door for production of the vast reserve of shale gas and shale oil, thus extending the world's energy prospect. The practice of fracking, however, is controversial as it creates many environmental concerns [117].

1.3.9 Water Wave and Seabed Interaction

Sea bottom sediment is a porous medium. The rising and falling of water waves exerts a pressure on the bottom that drives a seepage flow into and out of the seabed, as well as deforms it. This seepage is a viscous flow; hence it dissipates the energy of the propagating water wave, causing the wave to dampen. This problem has been investigated by assuming that the flow in the seabed satisfies Darcy's law [152, 195, 199].

Based on the simplest model [195], the dynamic pressure at the sea bottom is given by the linear water wave theory of a harmonic, small amplitude wave propagating over constant water depth, as

$$p = P_o \cos(\ell x - \omega t) \tag{1.73}$$

where P_o is the pressure magnitude, ℓ is the wave number, and ω is the wave frequency. This cycling pressure, changing from positive to negative, is added to the hydrostatic pressure proportional to the water depth. The flow in the seabed is modeled as a Darcy flow of incompressible fluid, governed by the Laplace equation

$$\frac{\partial^2 p}{\partial x^2} + \frac{\partial^2 p}{\partial z^2} = 0 \tag{1.74}$$

where z is pointing downward in the depth direction. Solution of (1.74), subject to the boundary condition (1.73) prescribed at $z = 0$, is

$$p(x, z, t) = P_o \, e^{-\ell z} \cos(\ell x - \omega t) \tag{1.75}$$

The above equation shows that the pore pressure in the seabed decays exponentially with depth, with a decay length characterized by the wavelength of the water wave; that is, the longer the water wave, the deeper the pore pressure penetration.

The curiosity of the above solution is that the pore pressure response is not dependent on any physical parameters of the seabed, not even the permeability. Also, the periodic response is completely in phase with the water wave at any depth. These are not realistic conditions. In other attempts, the seabed was modeled either as a fluid (mud) [58, 94], or as an elastic material without fluid [159]. These models are also physically deficient.

In a better approach, the seabed has been modeled as a poroelastic material. The resultant pore pressure is found to be dependent on a number of seabed physical parameters, such as permeability, compressibility of pore water, as well as that of the porous skeleton [156, 265]. Interestingly, it is demonstrated that the solution (1.75) is the limiting case of the poroelastic solution, if the pore water is considered to be incompressible ($C_f = 0$) [265], or if the permeability coefficient is taken to be infinite ($\kappa \to \infty$) [45]. In fact, (1.75) is the upper bound of pore pressure responses. That is, with a finite permeability or fluid compressibility, the pore pressure response is always smaller than that predicted by (1.75). Also, the cyclic response is increasingly off-phase going into depth.

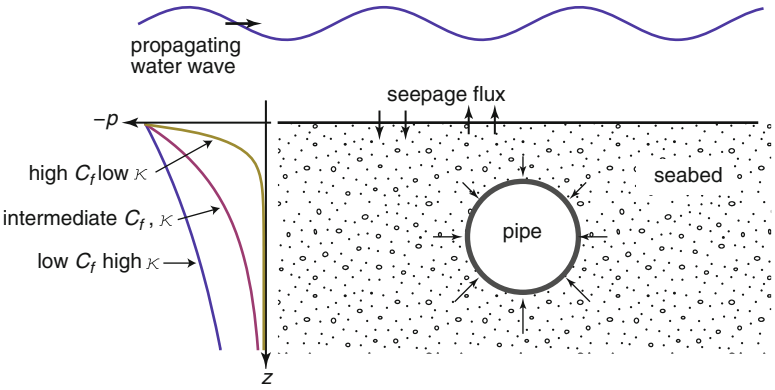

Fig. 1.11 Uplift force on a pipeline buried in sea bed

The poroelastic solution also shows that for small permeability or large pore water compressibility, the pressure penetration is limited to a surface layer; that is, there is a sharp drop-off within a small distance. It is of interest to comment that although seawater is considered nearly incompressible as compared to the sediment frame, a very small amount of entrapped gas can make it highly compressible. It is observed that recently deposited sediment often contains organic contents that can generate undissolved gas. For example, as much as 10 % by volume of undissolved gas was found in the submarine sediment of Mississippi Delta [14]; so the apparent pore water compressibility can be very large.

Next, consider a pipeline buried in the seabed (Fig. 1.11). The wave induced pore pressure has a gradient; hence creates a pressure differential on the upper and lower part of the pipe, resulting a net force. This dynamic buoyancy force pushes the pipe up and down, as well as left and right. Particularly, at the passage of wave trough, there is a uplift force. During a storm event, the upward dynamic buoyancy force can be large enough to overcome the overburden weight of the backfill to cause flotation of the pipeline [45, 131, 157]. Such force needs to be taken into design considerations.

As mentioned above, the penetration of pore pressure is strongly affected by the permeability of sediment, κ, and the (apparent) compressibility of water, C_f. In Fig. 1.11 we illustrate three pore pressure profiles corresponding to the large κ or small C_f, small κ or large C_f, and the intermediate κ and C_f case. If permeability is small or compressibility of water is large (right profile), the dynamic pore pressure drops off rapidly such that it does not penetrate to the depth of the pipeline; hence the pipe experiences very little uplift force. For large permeability and small pore water compressibility (left profile), the pore pressure response is the largest. However, buoyancy is generated not by the pressure itself, but by its differential at the top and bottom of the object. If the pressure profile is flat around where the pipeline is,

the buoyancy is also small. These cases lead to the interesting conclusion that the uplift force is largest at certain intermediate permeability and water compressibility values [45].

Other seabed related poroelastic phenomena include submarine slope instability and landslide [11, 114, 197], liquefaction [123, 210, 215], stability of breakwater [120, 130, 132], lifting of objects resting on seabed [87], and flux exchange between ocean and sediment as a mechanism of pollutant transport [133, 172, 193]. Another sediment related phenomenon is the damping of earthquake excitation in a dam-reservoir system by bottom sediment [40, 76].

1.3.10 Tidal and Barometric Efficiency

Gaius Plinius Secundus (AD 23–79), better known as Pliny the Elder, seems to be the first to observe that the water level in a coastal well responds to the rise and fall of ocean tide. In his book *Historia Naturalis* (Natural History), he stated that near the temple of Hercules in Cadiz "*there is a closed source similar to a well which occasionally rises and falls with the ocean*" [167].

In 1902, the United States Geological Survey reported that water level oscillations in wells in Atlantic City, New Jersey, were synchronous with the tidal cycle. The sea bottom pressure driven porous medium flow was ruled out as the cause, because the transmission of pore pressure by such flow would have a large time lag. Hence this effect was attributed to the weight of seawater compressing on the aquifer below, resulting an instant pore pressure rise, forcing the water level in the wells to go up [166].

Earth tide is the motion of the Earth's surface at periods of about 12 h and longer, due to the pull by gravity of the Moon and the Sun. Klonne in 1880 [144] reported on water level fluctuations in a flooded coal mine near Duchov, Czechoslovakia, and theorized that it was caused by the dilation produced by the Earth tide. According to Grablovitz [101] (translated):

> *It is known that the terrible catastrophe occurred February 10, 1879 at Dux, under which five large coal mines were flooded almost completely.*
>
> *He was reflecting on the means best adapted to repair that damage, when the director Mr. F. W. Klonne, mountain engineer, was made aware that the water level was not increasing continuously, as he had first thought, but decreased, and sometimes arrested for a few hours, and then increased with greater vigor.*
>
> *Being warned of this, the intelligent director did not take long to recognize that the fluctuations were due no less than the movement of ebb and flow, just as in the seas, of the lunar-solar attraction. He was so impressed that it did not take long for him to undertake, with a fervor worthy of anyone's praise, regular hourly observations, which began at 6 am of April 8 following the disaster, announced at the same time to the Academy of Sciences in Vienna, . . . and observations continued until 6 am of September 11, the day when the work on the extraction of water from flooded mines began . . .*

Other early observations of Earth tide induced water level fluctuation in wells include Young [273], Robinson [204], and Theis [241].

King in 1892 [143] reported that a heavily loaded moving train had the power of disturbing the water level in a well 140 ft away from the train station at Whitewater, Wisconsin. It was observed that with the passage of a train, there was "*a rapid but gradual rise of the water, which is followed by only a slightly less rapid fall again to the normal level, there being nothing oscillatory in character*." He reasoned that this phenomenon could not be explained by an elastic shock wave, because "*there is one single rise and fall, with no trace whatever in the curve of a repetition, as a true wave implies*."

In the same report, King also pored over the phenomenon of groundwater level fluctuation coinciding with the barometric pressure changes. He stated: "*a rise in the barometer is very nearly coincident in time with a fall of the water in wells and with a diminished rate of discharge of water from the ground, and vice versa*."

The ocean tide can also exert a periodic loading on the seafloor. Jupp and Schultz [137] presented a theory that the magnitude and phase of the temperature and flow rate of the seafloor *hydrothermal vent* are modulated by the changing weight of water column loaded on the seafloor.

From the poroelasticity theory, we realize that the ratio of the water surface rise in the well to the tidal level rise is given by the uniaxial Skempton pore pressure coefficient defined in (1.21), and is called the tidal efficiency [75, 126], denoted as γ_{te}. Utilizing the relations (1.12), (1.21), (1.23), and (1.46), and eliminating a few parameters, we obtain

$$\gamma_{te} = 1 - \frac{\phi}{SK_f} \tag{1.76}$$

The above equation suggests that if we obtain tidal efficiency from observation, and know the values of K_f and ϕ, we can estimate the storage coefficient S, which in turn is tied to the specific storativity of the aquifer as $S_s = \gamma_f S$ (see Sect. 1.2.6).

Similarly, we can define a *barometric efficiency* as the ratio of the pressure rise in the water well, calculated as $\Delta p = \gamma_f \Delta h$, to the change in atmospheric pressure, as

$$\gamma_{be} = \frac{\phi}{SK_f} \tag{1.77}$$

The reason that the above expression is different from (1.76) is because the atmospheric load exerts a pressure not only on the aquifer, but also on the water column in the well. So based on the observation of water level fluctuation in water well penetrating into an artisan aquifer, and the barometer record, the specific storativity of the aquifer can be estimated.

There are many applications that utilize the ocean, atmospheric, and Earth tide for the estimation of formation properties. Making the assumption that stresses associated with Earth tides act horizontally, and that the Earth is free to deform in the vertical direction, Bredehoeft [29] provided a method for estimating the storage coefficient of the aquifer from the magnitude of the water level change in a well, if the Poisson ratio of the formation is known. Further utilizing the phase shift of the water level response, the aquifer transmissivity can be determined [119].

Analyzing both the Earth and atmospheric tide effects, van der Kamp and Gale [252] presented formulas for the determination of the shear and bulk modulus, as well as porosity, of the formation. By filtering and separating the tidal data into high, intermediate, and low frequency responses, various aquifer parameters, such as well radius, lateral and vertical diffusivity, storativity, thickness of the unsaturated zone, vertical pneumatic diffusivity, etc., can be estimated [207].

Using the simple aquifer theory, Ferris in 1952 [84] suggested that the combined aquifer parameter T/S, where T is transmissivity and S storativity, can be determined from the data of water level fluctuation in wells, caused by the cyclic ocean tidal or stream stage loading. The theory was tested on stream stage fluctuation. The utilization of the ocean tidal effect for the determination of aquifer parameters was attempted by Erskine [81], as well as others [135, 169]. Similar technique was developed by Pinder et al. [188] using the recession limb of river flood stage.

1.3.11 Biomechanics

As cited in the prologue of this chapter, Leonardo da Vinci drew an analogy between the Earth and the human body, both as porous materials: "*Its flesh is the soil, its bones are the strata of rock, its cartilage is the tufa, its blood is the underground streams, the reservoir of blood around its heart is the ocean, the systole and diastole of the blood in the arteries and veins appear on the Earth as the rising and sinking of the oceans*". Biological materials, such as human and animal flesh, bones, cartilages, blood vessels, and plant tissues, are porous solid impregnated with fluid; hence should be studies as poroelastic materials, rather than solid or viscoelastic solid.

Compared with the lifeless rock, live cortical (compact) bone is a much more dynamic structure since it is under constant remodeling [274], meaning that bone tissue is removed from the skeleton and new bone tissue is formed, a process that can be stimulated by the stress loading. This seemingly dense matrix actually has several levels of porosity, which are filled with fluid. The fluid in the bone serves many functions. It transports nutrients to, and carries waste from, the bone cells (osteocytes) buried in the bony matrix. It is involved in the transport of mineral ions to the bone tissue for storage, and then for retrieval when they are needed by the body [54]. Bone deformation induced fluid flow causes the bone fluid to flow over the bone cell membrane. The shear stress of the flowing fluid is sensed by the cell, which has been suggested to have a role in bone's mechanosensory system [261].

Cartilage is a flexible connective tissue found in many parts of human body, such as in the joints between bones. It is a porous soft tissue impregnated with fluid. The viscous fluid flow in the pores gives the articular cartilage a viscoelastic-like behavior that serves as a damper to impact. It also provides a squeeze film lubrication with synovial fluid to prevent the solid surface from touching. The fluid exchange is a mechanism for nutrient transport [170, 171, 219].

Artery wall is the fibrous and muscular wall of vessels that carry oxygenated blood from the heart to structures throughout the body. A diseased vessel can get clogged by the deposit of low density lipoprotein (LDL), forming plaques,

and eventually becoming hardened, constricting the blood flow, and leading to the disease known as atherosclerosis. The inside of the artery wall is lined with a single layer of cells, known as endothelium. The onset of LDL deposit on the wall is often found at lesion site where the endothelial cells are torn off.

The artery wall is highly elastic [257], and it can inflate or contract with the high or low blood pressure inside the vessel. The higher intraluminal pressure drives a fluid flow through the wall, bringing nutrient, oxygen and macromolecules to the tissue [151, 230]. As the wall itself is infiltrated with fluid, the stretching and collapsing of the wall can respectively cause pressure drop and rise inside the wall. Particularly, with a sudden drop of intraluminal pressure, the contraction of the wall causes a sudden fluid pressure rise inside the artery wall, which in turn drives a flux both ways, toward the tissue, and toward the lumen. This reversal of flux toward lumen is suspected to be large enough to dislodge the endothelial cell, to be torn away by the shear force of the blood flow [46, 140]. Other scenarios of poroelastic effect on blood vessels include the rupture of abdominal aortic aneurysm when the artery wall stress exceeds that of the local wall strength [191].

Other biological tissues modeled as poroelastic material include ligament [7, 270], intervertebral disk [5, 223], cardiac tissue [39, 267], subcutaneous tissue [158, 264], and human brain [164].

1.3.12 Poroviscoelasticity and Anelastic Strain Recovery

The hydraulic fracturing technique described in the preceding section is the most reliable method for the determination of the magnitude of in situ stress. It is, however, costly to perform. Also, as the breakdown of borehole is initiated when the minimum in situ stress is reached, this technique can only measure the minimum, and not the maximum, in situ stress.

An alternative technique can be devised based on the strain relaxation phenomenon of cylindrical cores retrieved at great depths. Once the confining stress is removed from a retrieved core, it starts to slowly expand, typical of a *viscoelastic* material. This creep behavior can be attributed to several physical mechanisms, such as the intergranular frictional sliding, the intrinsic solid grain creep deformation, and the solid-fluid interactions in fissures at the sub-granular scale [21, 48]. However, sometimes the core is observed to contract, before it expands. This non-monotonic behavior can only be explained by the interaction between the poroelastic and viscoelastic effects.

This *anelastic strain recovery* (ASR) method [56, 258] has been used as one of the lower cost techniques for determining the in situ stresses. In the practice, a drill core is quickly retrieved to the ground (within several hours), immediately instrumented with displacement gages, and then monitored for strain relaxation for 1–3 days. With a valid viscoelastic constitutive model, this technique can be used to determine not only the directions, but also the magnitude of in situ stresses [24, 240, 259].

When we construct a constitutive model for the retrieved cores, we need to be aware that rocks are not only viscoelastic, but also poroelastic. As both of these mechanisms are time dependent, when we rely on the transient data to determine the in situ stress, a model cannot ignore one or the other. These two mechanisms each have their own response time. The characteristic time of viscoelastic behavior is a material property. In fact, as described above, there exist several transient physical mechanisms, such that several characteristic times may be needed to even model the viscoelastic responses. However, for a particular application, such as ASR, only characteristic times falling within a range of time of interest, such as from a few hours to a few days, need to be considered.

The poroelastic response, although transient, should not be modeled as a viscoelastic one [30], as the poroelastic characteristic time is dependent not only on the material itself, but also on the geometry of the specimen. As discussed in Sect. 1.2.2, the characteristic time of a poroelastic specimen can be estimated as $t_c = L_c^2/c$, where c is the consolidation coefficient, and L_c is largest distance that the pore pressure diffusion front needs to travel, originating from a drainage surface to reach to the innermost part of the specimen. So the characteristic time is sensitive to the square of the size of the specimen. The consolidation coefficient is a material property; and particularly, it is directly proportional to the *intrinsic permeability* of the rock, k, which can range from 10^{-1} darcy for sandstone to 10^{-7} darcy for shale.

While the solid viscoelastic behavior predicts that material will expand after the removal of the confining stress, the actual core behavior is more complex. Some cores were observed to contract, and some contract and then expand, or the other way around [31, 74, 80, 260]. The contraction of the core can be easily explained by the poroelastic effect. Once the core is retrieved, if there is still a residual pore pressure within the core, it will have to dissipate with time. Based on the thermoelasticity analogy discussed in Sect. 1.2.7, pore pressure is equivalent to temperature. As a cylinder cools down, it contracts; the same effect is found in pore pressure dissipation. Another way to view this phenomenon is by the effective stress. As the cylinder is free from an external compressive stress, the existence of pore pressure effectively makes the core in tension. Once that tension disappears, the core contracts. The coexistence of the viscoelastic and poroelastic effects can create the non-monotonic behaviors observed in the drill cores. Such phenomena have been modeled using the poroviscoelasticity theory [1, 2].

1.3.13 Porothermoelasticity and Thermal Fracturing

In Sect. 1.2.7 we discussed that heat on an elastic solid is analogous to pore pressure on a poroelastic material assuming it is under isothermal condition, in terms of their deformation and stress responses. When heat is applied to a saturated poroelastic material, we have more complicated physical mechanisms to consider, as there exists the interaction of heat effect on two constituents, solid and fluid, which have different thermal expansion coefficients. The relative magnitude of these coefficients has an important consequence on material failure by effective stress.

Consider a porous specimen free from external stresses and subject to a uniform temperature rise. The sample will expand just as an elastic solid. For geomaterials saturated with water, the fluid thermal expansion coefficient is typically larger than that of the solid. If the fluid is not allowed or does not have time enough to escape, a pressure will develop inside the specimen due to the smaller expansion of the pore space. As there is no externally applied confining stress, this internal pressure pushes on the porous structure making it effectively in tension, as predicted by Terzaghi effective stress. Hence heating a saturated concrete to high temperature can make it to explode, known as *pore pressure spalling* [10, 57, 138, 186].

Now consider a different scenario—the porous specimen is restrained from deformation and is cooled. Both solid and fluid will contract. The contraction of solid makes it in tension. The fluid however contracts more, and a negative pressure will develop, which compensates the effective stress, making the solid less in tension. At large time, the pore pressure is dissipated, and the solid is in maximum tension. If the material is cooled enough, the solid can crack. This effect has been utilized as a *thermal fracturing* technique by the industry. In a geological formation cold fluid can be injected into a borehole or a fracture to lower the temperature on the wall to induce cracks. These thermally induced fracture zone can enhance the permeability of the formation for enhanced oil recovery, unconventional gas extraction, nuclear waste disposal, geothermal energy extraction, and CO_2 geosequestration [271].

1.3.14 Poroelastodynamics and Seismoelectric Effect

As early as in 1930s, geophysicists in the US have observed that the passage of a seismic wave, such as one that is generated by an underground explosion, creates a disturbance in an electric field [25]; that is, the current strength in the soil, in the presence of a constant potential difference between two electrodes, fluctuates under the influence of elastic vibrations. Thompson in 1936 [245] provided an explanation to the phenomenon as a change in earth resistivity due to the elastic deformation. This has been called as the *seismoelectric effect of the first kind*, or the *J-effect*.

In 1939, Ivanov [124, 125] in Russia reported that in moist soil, there is a *seismoelectric effect of the second kind*, or the *E-effect*. The second kind effect is characterized by an electrical potential generated within the earth without an externally applied electric field, by the passage of seismic waves, Also, this electric potential travels ahead of the seismic waves, in contrast with the effect of the first kind. In 1944, the famous Russian physicist Frenkel (see Sect. F.13 for a biography) proposed a mechanism based on the relative movement of solid and fluid containing electrolytes during the passage of a seismic wave. In that effort, he formulated the first theory of poroelastodynamics [92]. The theory was later refined by Biot [18, 19] (see Chap. 9).

Martner and Sparks in 1959 [161] suggested that the arrival of the seismoelectric pulse at ground level far away from the source of explosion is instant; hence

it must be due to the propagation of an electromagnetic wave. The detection of such electromagnetic wave in the field was reported by Thompson and Gist [243]. The governing equations for the seismoelectric-electromagnetic phenomenon were presented by Pride [194], which include the Maxwell equations. In fact, not only a seismic event can generate electric and electromagnetic fields, but also electric and electromagnetic pulses can generate seismic waves [244], which is called the *electroseismic effect*.

It is well known that in an elastic medium there exist two propagating waves, a compressional wave, also known as the P-wave, and a shear wave, known as the S-wave. In porous medium, it has been demonstrated by Frenkel [92] and Biot [18, 19] that due to the presence of a fluid phase, two compressional waves exist—a *compressional wave of the first kind* characterized by the in-phase motion of solid and fluid, and a *compressional wave of the second kind* due to the relative motion between the solid and fluid. The first wave is similar to an elastic wave, and called a *fast wave*, with a small amount of attenuation. The second wave is with a much slower propagation speed and highly dissipative, and is called a *slow wave*. The phase velocities of both waves are frequency dependent; hence these waves are *dispersive waves*.

Figure 1.12 illustrates the propagation of a second wave in which the solid and fluid move in opposite directions. In soils and geological formations the fluid often contains dissolved electrolytes. The positive charge on the solid surface and the negative charge in the fluid form electric double layers. Their relative motion generates local electric currents, which is the E-effect. The fluctuation of the electric current further generates electromagnetic waves. The seismoelectric and the electroseismic effects can be used in many applications, such as the detection of hydrocarbon in formation [244], exploration of fractures [277] and permeable zones [168] in boreholes, detection of horizontal bedding plane fractures in groundwater exploration [88], and tracking the underground NAPL contaminant front [201].

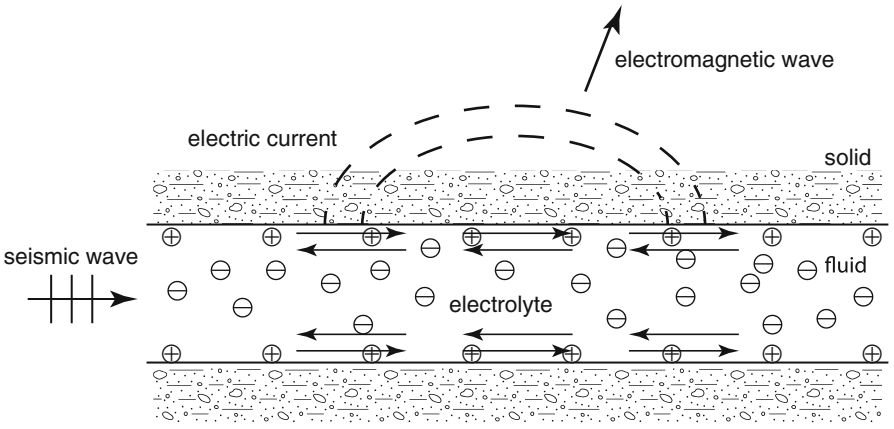

Fig. 1.12 Seismoelectric and seismoelectromagnetic effect

1.3.15 Swelling of Clay and Shale

It is well known that clay can swell by a large amount when it becomes wet, and contract and crack when it is dried. This drastic expansion and shrinkage behavior causes many construction problems, such as cracking of foundations and walls, and heaving of roadways. On the other hand, clay properties can also be used for beneficially purposes such as liner materials in the containment of waste [208] and catalytic materials [249].

The swelling of clay consists of two phases. In the *innercrystalline swelling*, water is taken up in a process called *hydration* for dry or partially saturated clay. Clay particles are in the form of platelets that stack together in multiple layers. In the fully dry montmorillonite, a dominant type of clay, the layers lie so close together that they are almost in contact. When in contact with water, the water molecules enter the interlayer space and bond with the cations and order themselves into single or multiple layers that repel the clay platelet, causing the swelling [115].

Once the clay becomes saturated, a second type of swelling can result from the difference in the ion concentration, and principally in the cation concentration, at the surface of the clay layers and in the pore water, known as *osmotic swelling*. The clay surface is negatively charged, which attracts positive ions surrounding it to form a diffuse electric double layer. This electric cloud behaves as a semi-permeable membrane is an osmosis process that allows the passage of water molecules yet blocks the charged ions. With the adsorbed water, the clay particles repel each other making it to swell, but to a much less extent than that of the hydration process.

Swelling of shale is of major problem for petroleum engineering. Shale makes up more than 75 % of drilled formations and causes at least 90 % of wellbore-stability problems [50]. Drilling in shale can result in a variety of problems, ranging from bit balling, sloughing, or creep, to washout and complete hole collapse. Although the use of oil based drilling mud can reduce the chemical effect, its use is much restricted due to the environmental concern of its disposal [254]. For the water based drilling mud, its chemistry can be controlled to minimize the osmotic effect, or even to utilize it for the stability of the shale. The difference in solute concentration between the drilling mud and the formation can create an osmotic pressure in the shale that plays a role in the extended effective stress concept, thus affecting the stability of the borehole wall. Some of these effects can be models by the *porochemoelasticity* theory as presented in Chap. 12.

1.3.16 Nanoporous Material

Nanoporous material is defined as materials with pore size of the order 100 nm or smaller [154]. Such materials are abundant in nature both in biological systems, such as cell membranes, and in natural minerals, such as activated carbon and zeolites. Nanoporous materials have been used in industry for various purposes for a long time. For example, zeolites are widely used for water purification and as catalysts.

However, only the recent emergence of nanotechnology allows us to realize the nanoscale nature of these materials, and the physico-chemical mechanisms that make them efficient. The invention of scanning tunneling microscope and atomic force microscope also enables us to see and manipulate materials at the nanoscale, opening the opportunity for designing and manufacturing new nanoporous materials for industrial, electronic, and biomedical applications.

Nanoporous materials can be classified as membrane and bulk materials. Membrane material works as a molecular sieve. Its nano sized pores allow the passage of only smaller size molecules, and blocks the larger ones. Its biological and medical applications involve sorting, sensing, isolating and releasing biological molecules [3]. The bulk materials are utilized for their large surface to volume ratios. For the same porosity, if we make the pores smaller and smaller, the pore surface area increases linearly as the pore size decreases. For example, one gram of activated carbon with pore size of a few nanometers can have as much as several hundred to one thousand square meters of surface area. Hence nanoporous materials can be highly effective for use as adsorbents and ion-exchangers in chemical industry, and for drug delivery in medical applications. The agricultural product biochar (a charcoal used for soil amendment) has been considered to have the potential as a carbon sequestration tool for reversing climate change, by adsorbing CO_2 onto its pore surface [150].

Many macroporous structural materials contain porosity at multiple scales. For example, cement is found to contain a hierarchy of pores, from mortar scale (10^{-3} m) to cement paste (10^{-4} m), to C-S-H (Calcium-Silicate-Hydrate) matrix (10^{-6} m), to C-S-H solid (17 nm), and to globules (2.5 nm or less) [53, 134]. Particularly, at the globules scale, the nanoporosity is estimated to be about 18 % [134, 233]. The multiscale concrete has been modeled as a microporomechanical material [248]. Through nanoindentation, it has been found that the packing density of the C-S-H is largely responsible for the strength and the large time creep of the concrete [162, 251]. Nano particles, such as graphene, have been added to modify cement's mechanical, thermal, and electrical properties [4]. This is indeed a developing area of poromechanics.

References

1. Abousleiman Y, Cheng AHD, Jiang C, Roegiers JC (1993) A micromechanically consistent poroviscoelasticity theory for rock mechanics applications. Int J Rock Mech Mining Sci 30(7):1177–1180
2. Abousleiman Y, Cheng AHD, Jiang C, Roegiers JC (1996) Poroviscoelastic analysis of borehole and cylinder problems. Acta Mech 119(1–4):199–219
3. Adiga SP, Jin C, Curtiss LA, Monteiro-Riviere NA, Narayan RJ (2009) Nanoporous membranes for medical and biological applications. Wiley Interdiscip Rev Nanomed Nanobiotechnol 1(5):568–581
4. Alkhateb H, Al-Ostaz A, Cheng AHD, Li XB (2013) Materials genome for graphene-cement nanocomposites. J Nanomech Micromech ASCE 3(3):67–77

5. Argoubi M, Shirazi-Adl A (1996) Poroelastic creep response analysis of a lumbar motion segment in compression. J Biomech 29(10):1331–1339
6. Atkinson C (1986) Steady pore pressure profiles associated with a moving trench. Int J Eng Sci 24(10):1681–1695
7. Atkinson TS, Haut RC, Altiero NJ (1997) A poroelastic model that predicts some phenomenological responses of ligaments and tendons. J Biomech Eng ASME 119(4):400–405
8. Banhart J (2001) Manufacture, characterisation and application of cellular metals and metal foams. Prog Mater Sci 46(6):559–632
9. Barksdale HC, Sundstrom RW, Brunstein MS (1936) Supplementary report on the groundwater supplies of the Atlantic City region. New Jersey State Water Policy Commission Special Report 6, 139pp
10. Bažant ZP, Thonguthai W (1979) Pore pressure in heated concrete walls–theoretical prediction. Mag Concr Res 31(107):67–76
11. Bea RG, Wright SG, Sircar P, Niedoroda AW (1983) Wave-induced slides in south pass block 70, Mississippi Delta. J Geotech Eng ASCE 109(4):619–644
12. Beamish BB, Crosdale PJ (1998) Instantaneous outbursts in underground coal mines: an overview and association with coal type. Int J Coal Geol 35(1–4):27–55
13. Bear J, Cheng AHD (2010) Modeling groundwater flow and contaminant transport. Springer, Dordrecht/London, 834pp
14. Bennett RH, Faris JR (1979) Ambient and dynamic pore pressures in fine-grained submarine sediments: Mississippi Delta. Appl Ocean Res 1(3):115–123
15. Berchenko I, Detournay E (1997) Deviation of hydraulic fractures through poroelastic stress changes induced by fluid injection and pumping. Int J Rock Mech Mining Sci 34(6):1009–1019
16. Biot MA (1941) General theory of three-dimensional consolidation. J Appl Phys 12(2):155–164
17. Biot MA (1956) Thermoelasticity and irreversible thermodynamics. J Appl Phys 27(3):240–253
18. Biot MA (1956) Theory of propagation of elastic waves in a fluid-saturated porous solid. 1. Low-frequency range. J Acoust Soc Am 28(2):168–178
19. Biot MA (1956) Theory of propagation of elastic waves in a fluid-saturated porous solid. 2. Higher frequency range. J Acoust Soc Am 28(2):179–191
20. Biot MA (1959) New thermomechanical reciprocity relations with application to thermal stress analysis. J Aerosp Sci 26(7):401–408
21. Biot MA (1962) Mechanics of deformation and acoustic propagation in porous media. J Appl Phys 33(4):1482–1498
22. Biot MA (1963) Science and the engineer. Appl Mech Rev 16(2):89–90
23. Biot MA, Willis DG (1957) The elastic coefficients of the theory of consolidation. J Appl Mech ASME 24:594–601
24. Blanton TL (1983) The relation between recovery deformation and *in-situ* stress magnitudes. In: SPE/DOE low permeability gas reservoirs symposium, Denver
25. Blau LW, Statham L (1936) Method and apparatus for seismicelectric prospecting. U.S. Patent 2054067
26. Bluhm J, de Boer R (1996) Effective stresses—a clarification. Arch Appl Mech 66(7):479–492
27. Boley BA, Weiner JH (1960) Theory of thermal stresses. Wiley, New York, 586pp
28. Booker JR (1974) Time dependent strain following faulting of a porous medium. J Geophys Res 79(14):2037–2044
29. Bredehoeft JD (1967) Response of well-aquifer systems to Earth tides. J Geophys Res 72(12):3075–3087
30. Brereton NR, Chroston PN, Evans CJ (1995) Pore pressure as an explanation of complex anelastic strain recovery results. Rock Mech Rock Eng 28(1):59–66

31. Brereton NR, Chroston PN, Evans CJ, Hudson JA, Whitmarsh RB (1992) Anelastic strain recovery and elastic properties of oceanic basaltic rocks. In: Gradstein FM, Ludden JN et al (eds) Proceedings of the ocean drilling program. Scientific results, vol 123. Ocean Drilling Program, College Station, pp 469–491
32. Bridgman PW (1912) Breaking tests under hydrostatic pressure and conditions of rupture. Philos Mag 24(139):63–80
33. Brown DW (2000) A hot dry rock geothermal energy concept utilizing supercritical CO_2 instead of water. In: Proceedings of the 25th workshop on geothermal reservoir engineering, SGP-TR-165, Stanford University, Stanford
34. Bruno MS, Nakagawa FM (1991) Pore pressure influence on tensile fracture propagation in sedimentary rock. Int J Rock Mech Mining Sci 28(4):261–273
35. Burke M, Kingsbury HB (1984) Response of poroelastic layers to moving loads. Int J Solids Struct 20(5):499–511
36. Carder DS (1945) Seismic investigations in the Boulder Dam area, 1940–1944, and the influence of reservoir loading on earthquake activity. Bull Seismol Soc Am 35:175–192
37. Chan DYC, Hughes BD, Paterson L (1993) Transient gas flow around boreholes. Trans Porous Media 10(2):137–152
38. Chan DYC, Hughes BD, Paterson L (1993) Tensile stresses around boreholes due to transient fluid flow. Int J Numer Anal Methods Geomech 17(9):659–667
39. Chapelle D, Gerbeau JF, Sainte-Marie J, Vignon-Clementel IE (2010) A poroelastic model valid in large strains with applications to perfusion in cardiac modeling. Comput Mech 46(1):91–101
40. Cheng AHD (1986) Effect of sediment on earthquake-induced reservoir hydrodynamic response. J Eng Mech ASCE 112(7):654–665
41. Cheng AHD (2000) Multilayered aquifer systems—fundamentals and applications. Marcel Dekker, New York/Basel, 384pp
42. Cheng AHD, Abousleiman Y, Roegiers JC (1993) Review of some poroelastic effects in rock mechanics. Int J Rock Mech Mining Sci 30(7):1119–1126
43. Cheng AHD, Badmus T, Beskos DE (1991) Integral equation for dynamic poroelasticity in frequency domain with BEM solution. J Eng Mech ASCE 117(5):1136–1157
44. Cheng AHD, Liggett JA (1984) Boundary integral equation method for linear porous-elasticity with applications to fracture propagation. Int J Numer Methods Eng 20(2):279–296
45. Cheng AHD, Liu PLF (1986) Seepage force on a pipeline buried in a poroelastic seabed under wave loadings. Appl Ocean Res 8(1):22–32
46. Cheng AHD, Skalak R, Weinbaum S, Ni JCY (1984) Consolidation of poroelastic arterial tissue. In: Boresi AP, Chong KP (eds) Engineering mechanics in civil engineering, proceedings of the 5th ASCE/EMD specialty conference. University of Wyoming, Laramie, pp 891–894
47. Clark JB (1949) A hydraulic process for increasing the productivity of wells. Trans Am Inst Mining Metall Eng 186(1):1–8
48. Cleary MP (1978) Elastic and dynamic response regimes of fluid-impregnated solids with diverse microstructures. Int J Solids Struct 14(10):795–819
49. Cleary MP (1978) Moving singularities in elasto-diffusive solids with applications to fracture propagation. Int J Solids Struct 14(2):81–97
50. Cleary MP (1980) Analysis of mechanisms and procedures for producing favourable shapes of hydraulic fractures. In: SPE annual technical conference and exhibition, Dallas
51. Cleary MP (1980) Comprehensive design formulae for hydraulic fracturing. In: SPE annual technical conference and exhibition. Dallas
52. Cocco M, Rice JR (2002) Pore pressure and poroelasticity effects in Coulomb stress analysis of earthquake interactions. J Geophys Res Solid Earth 107(B2):2030
53. Constantinides G, Ulm FJ (2004) The effect of two types of C-S-H on the elasticity of cement-based materials: results from nanoindentation and micromechanical modeling. Cem Concr Res 34(1):67–80
54. Cowin SC (1999) Bone poroelasticity. J Biomech 32(3):217–238
55. Cryer CW (1963) A comparison of the three-dimensional consolidation theories of Biot and Terzaghi. Q J Mech Appl Math 16(4):401–412

56. Dally JW, Riley WF (1978) Experimental stress analysis. McGraw-Hill, New York, 571pp
57. Dal Pont S, Colina H, Dupas A, Ehrlacher A (2005) An experimental relationship between complete liquid saturation and violent damage in concrete submitted to high temperature. Mag Concr Res 57(8):455–461
58. Dalrymple RA, Liu PLF (1978) Waves over soft muds: a two-layer fluid model. J Phys Oceanogr 8(6):1121–1131
59. David EC, Zimmerman RW (2011) Compressibility and shear compliance of spheroidal pores: exact derivation via the Eshelby tensor, and asymptotic expressions in limiting cases. Int J Solids Struct 48(5):680–686
60. Davies GH, Reynolds SJ (1996) Structural geology of rocks and regions, 2nd edn. Wiley, New York, 776pp
61. da Vinci L (1506–1510) Codex leicester
62. Davis SD, Pennington WD (1989) Induced seismic deformation in the Cogdell oil-field of West Texas. Bull Seismol Soc Am 79(5):1477–1494
63. de Boer R (2000) Theory of porous media, highlights in the historical development and current state. Springer, Berlin/New York, 618pp
64. de Boer R (2005) The engineer and the scandal: a piece of science history. Springer, Berlin/Heidelberg, 293pp
65. de Boer R, Ehlers W (1988) A historical review of the formulation of porous media theories. Acta Mech 74(1–4):1–8
66. de Boer R, Ehlers W (1990) The development of the concept of effective stresses. Acta Mech 83(1–2):77–92
67. de Laguna W (1966) Disposal of radioactive wastes by hydraulic fracturing: part I. General concept and first field experiments. Nucl Eng Design 3(2):338–352
68. de Laguna W (1966) Disposal of radioactive wastes by hydraulic fracturing: part II. Mechanics of fracture formation and design of observation and monitoring wells. Nucl Eng Design 3(3):432–438
69. Deresiewicz H, Skalak R (1963) On the uniqueness in dynamic poroelasticity. Bull Seismol Soc Am 53(4):783–788
70. Detournay E, Cheng AHD (1988) Poroelastic response of a borehole in a non-hydrostatic stress field. Int J Rock Mech Mining Sci 25(3):171–182
71. Detournay E, Cheng AHD (1991) Plane strain analysis of a stationary hydraulic fracture in a poroelastic medium. Int J Solids Struct 27(13):1645–1662
72. Detournay E, Cheng AHD (1992) Influence of pressurization rate on the magnitude of the breakdown pressure. In: Tillerson JR, Wawersik WR (eds) Rock mechanics, proceedings of the 33rd U.S. symposium, Balkema, pp 325–333
73. Detournay E, Cheng AHD, Roegiers JC, McLennan JD (1989) Poroelasticity considerations in *in-situ* stress determination by hydraulic fracturing. Int J Rock Mech Mining Sci 26(6):507–513
74. Dey TN, Kranz RL (1988) State of stress and relationship of mechanical properties to hydrothermal alteration at valles caldera core hole 1, New Mexico. J Geophys Res Solid Earth Planets 93(B6):6108–6112
75. Domenico PA (1983) Determination of bulk rock properties from ground-water level fluctuations. Bull Assoc Eng Geol 83(3):283–287
76. Domínguez J, Gallego R, Japón BR (1997) Effects of porous sediments on seismic response of concrete gravity dams. J Eng Mech ASCE 123(4):302–311
77. Dreesen DS, Nicholson RW (1985) Well completion and operations for MHF of Fenton Hill well EE-2. Geotherm Resour Counc Trans Part 2 9:105–110
78. Dropek RK, Johnson JN, Walsh JB (1978) Influence of pore pressure on mechanical properties of Kayenta sandstone. J Geophys Res 83(NB6):2817–2824
79. Economides MJ, Nolte KG (eds)(2000) Reservoir stimulation, 3rd edn. Wiley, Chichester/New York, 856pp
80. El Rabaa AW, Meadows DL (1986) Laboratory and field application of the strain relaxation method, SPE 15072, SPE 56th California regional meeting, Oakland, pp 259–272

81. Erskine AD (1991) The effect of tidal fluctuation on a coastal aquifer in the UK. Ground Water 29(4):556–562
82. Fairhurst C (1964) Measurement of *in situ* rock stresses, with particular reference to hydraulic fracturing. Rock Mech Eng Geol 2:129–147
83. Fam MA, Dusseault MB, Fooks JC (2003) Drilling in mudrocks: rock behavior issues. J Pet Sci Eng 38(3–4):155–166
84. Ferris JG (1952) Cycle fluctuation of water levels as a basis for determining aquifer transmissibility, Groundwater Note 1, U.S. Geological Survey, Washington, DC
85. Figueroa JD, Fout T, Plasynski S, McIlvried H, Srivastava RD (2008) Advances in CO2 capture technology—the U.S. Department of Energy's carbon sequestration program. Int J Greenh Gas Control 2(1):9–20
86. Fillunger P (1936) Erdbaumechanik? (Earthwork Mechanics?). Wien: Selbstverlag des Verfassers (Vienna: self published by author)
87. Foda MA (1982) On the extrication of large objects from the ocean bottom (the breakout phenomenon). J Fluid Mech 117:211–231
88. Fourie F (2006) Aspects of the lateral and vertical resolution of surface electroseismic data with implications for groundwater exploration in fractured Karoo rocks. S Afr J Geol 109(4):571–584
89. Frank U, Barkley N (1995) Remediation of low permeability subsurface formations by fracturing enhancement of soil vapor extraction. J Hazard Mater 40(2):191–201
90. Franke PR, Nunz GJ (1985) Recent developments in the hot dry rock geothermal energy program. Geotherm Resour Counc Trans Part 2 9:95–98
91. Freed AM (2005) Earthquake triggering by static, dynamic, and postseismic stress transfer. Ann Rev Earth Planet Sci 33:335–367
92. Frenkel J (1944) On the theory of seismic and seismoelectric phenomena in moist soil. J Phys USSR 13(4):230–241
93. Fung YC (1977) A first course in continuum mechanics, 2nd edn. Prentice-Hall, Englewood Cliffs, 351pp
94. Gade HS (1957) Effects of a non-rigid, impermeable bottom on plane surface waves in shallow water. J Marine Res 16:61–82
95. Gambolati G, Teatini P (2014) Venice shall rise again: engineered uplift of Venice through saltwater injection. Elsevier, London/Waltham, 83pp
96. Garg SK, Nur A (1973) Effective stress laws for fluid-saturated porous rocks. J Geophys Res 78(26):5911–5921
97. Gassmann F (1951) Über die elastizität poröser medien (On elasticity of porous media). Veirteljahrsschrift der Naturforschenden Gesellschaft in Zürich 96:1–23
98. Geertsma J (1957) A remark on the analogy between thermoelasticity and the elasticity of saturated porous media. J Mech Phys Solids 6(1):13–16
99. Gibson RE, Knight K, Taylor PW (1963) A critical experiment to examine theories of three dimensional consolidation. In: Proceedings, European conference on soil mechanics and foundation engineering, vol 1, Weisbaden, pp 69–76
100. Gough DI, Bell JS (1982) Stress orientations from borehole wall fractures with examples from Colorado, east Texas, and northern Canada. Canad J Earth Sci 19(7):1358–1370
101. Grablovitz G (1880) Sul fenomeno di marea osservato nelle miniere di Dun in Bohemia (On the phenomenon of tide observed in the mines of Dun in Bohemia). Bull della Soc Adriat di Sci Nat Trieste 6:24–50
102. Gupta HK (1992) Reservoir-induced earthquakes. Elsevier, Amsterdam/New York, 364pp
103. Gupta HK (2002) A review of recent studies of triggered earthquakes by artificial water reservoirs with special emphasis on earthquakes in Koyna, India. Earth Sci Rev 58(3–4):279–310
104. Gutierrez MS, Lewis RW (2002) Coupling of fluid flow and deformation in underground formations. J Eng Mech ASCE 128(7):779–787
105. Haimson BC (1978) The hydrofracturing stress measuring method and recent field results. Int J Rock Mech Mining Sci 15(4):167–178

106. Haimson B, Fairhurst C (1967) Initiation and extension of hydraulic fractures in rocks. Soc Pet Eng J 7:310–318
107. Haimson B, Fairhurst C (1969) Hydraulic fracturing in porous-permeable materials. J Pet Technol 21:811–817
108. Haimson BC, Rummel F (1982) Hydrofracturing stress measurements in the Iceland research drilling project drill hole at Reydarfjordur, Iceland. J Geophys Res 87(NB8):6631–6649
109. Handin J, Hager RV, Friedman M, Feather JN (1963) Experimental deformation of sedimentary rock under confining pressure: pore pressure effects. AAPG Bull 47:717–755
110. Hantush MS, Jacob CE (1955) Non-steady radial flow in an infinite leaky aquifer. Trans Am Geophys Union 36(1):95–100
111. Hashin Z, Shtrikman S (1961) Note on a variational approach to the theory of composite elastic materials. J Frankl Inst Eng Appl Math 271(4):336–341
112. Hayashi K, Haimson BC (1991) Characteristics of shut-in curves in hydraulic fracturing stress measurements and determination of *in situ* minimum compressive stress. J Geophys Res 96(B11):18311–18321
113. Healy JH, Rubey WW, Griggs DT, Raleigh CB (1968) Denver earthquakes. Science 161(3848):1301–1310
114. Henkel DJ (1970) Role of waves in causing submarine landslides. Géotechnique 20(1):75–80
115. Hensen EJM, Smit B (2002) Why clays swell. J Phys Chem B 106(49):12664–12667
116. Howard GC, Fast CR (1970) Hydraulic fracturing. Society of Petroleum Engineers, New York, 203pp
117. Howarth RW, Ingraffea A, Engelder T (2011) Natural gas: should fracking stop? Nature 477(7364):271–275
118. Hsieh PA, Bredehoeft JD (1981) A reservoir analysis of the Denver earthquakes—a case of induced seismicity. J Geophys Res 86(NB2):903–920
119. Hsieh PA, Bredehoeft JD, Farr JM (1987) Determination of aquifer transmissivity from Earth tide analysis. Water Resour Res 23(10):1824–1832
120. Hsu JRC, Jeng DS, Tsai CP (1993) Short-crested wave-induced soil response in a porous seabed of infinite thickness. Int J Numer Anal Methods Geomech 17(8):553–576
121. Hubbert MK, Rubey WW (1959) Role of fluid pressure in mechanics of overthrust faulting. 1. Mechanics of fluid-filled porous solids and its application to overthrust faulting. Geol Soc Am Bull 70(2):115–166
122. Hubbert MK, Willis DG (1957) Mechanics of hydraulic fracturing. Trans Am Inst Mining Eng 210:153–166
123. Ishihara K, Yamazaki A (1984) Analysis of wave-induced liquefaction in seabed deposit of sand. Soil Found 24(3):85–100
124. Ivanov AG (1939) Effect of electrization of earth layers by elastic waves passing through them. Dokl Akad Nauk SSSR 24(1):42–45
125. Ivanov AG (1940) The electroseismic effect of the second kind. Izv Akad Nauk SSSR Ser Geogr Geofiz 5:699–727
126. Jacob CE (1940) On the flow of water in an elastic artesian unconfined aquifer. Trans Am Geophys Union 21:574–586
127. Jaeger JC (1963) Extension failures in rocks subject to fluid pressure. J Geophys Res 68(21):6066–6067
128. Jaeger JC, Cook NGW (1963) Pinching-off and disking of rocks. J Geophys Res 68(6):1759–1765
129. Jaeger JC, Cook NGW, Zimmerman C (2007) Fundamentals of rock mechanics, 4th edn. Wiley-Blackwell, Malden, 488pp
130. Jeng DS (1997) Wave-induced seabed instability in front of a breakwater. Ocean Eng 24(10):887–917
131. Jeng DS (2001) Numerical modeling for wave-seabed-pipe interaction in a non-homogeneous porous seabed. Soil Dyn Earthq Eng 21(8):699–712
132. Jeng DS (2001) Mechanism of the wave-induced seabed instability in the vicinity of a breakwater: a review. Ocean Eng 28(5):537–570

133. Jeng DS, Barry DA, Li L (2001) Water wave-driven seepage in marine sediments. Adv Water Resour 24(1):1–10
134. Jennings HM (2000) A model for the microstructure of calcium silicate hydrate in cement paste. Cem Concr Res 30(1):101–116
135. Jiao JJ, Tang Z (1999) An analytical solution of groundwater response to tidal fluctuation in a leaky confined aquifer. Water Resour Res 35(3):747–751
136. Jónsson S, Segall P, Pedersen R, Björnsson G (2003) Post-earthquake ground movements correlated to pore-pressure transients. Nature 424(6945):179–183
137. Jupp TE, Schultz A (2004) A poroelastic model for the tidal modulation of seafloor hydrothermal systems. J Geophys Res Solid Earth 109(B3):B03105
138. Kalifa P, Menneteau F-D, Quenard D (2000) Spalling and pore pressure in HPC at high temperatures. Cem Concr Res 30(12):1915–1927
139. Kehle RO (1964) The determination of tectonic stresses through analysis of hydraulic well fracturing. J Geophys Res 69(2):259–273
140. Kenyon DE (1979) Mathematical model of water flux through aortic tissue. Bull Math Biol 41(1):79–90
141. Kim JM, Parizek RR (1997) Numerical simulation of the Noordbergum effect resulting from groundwater pumping in a layered aquifer system. J Hydrol 202(1–4):231–243
142. Kim JM, Parizek RR (2005) Numerical simulation of the Rhade effect in layered aquifer systems due to groundwater pumping shutoff. Adv Water Resour 28(6):627–642
143. King FH (1892) Fluctuations in the level and rate of movement of ground-water on the Wisconsin Agricultural Experiment Station Farm and at Whitewater, Wisconsin. Bulletin No. 5. U.S. Department of Agriculture, Washington, DC, 75pp
144. Klonne FW (1880) Die periodischen schwankungen des wasserspiegels in den inundieten kohlenschachten von Dux in der period von 8 April bis 15 September 1879 (The periodic fluctuations of water levels in the flooded coal mine at Dux in the period 8 April to 15 September 1879). Sitzungsberichte Kaiserliche Akademie der Wissenschaften in Wien
145. Lade PV, de Boer R (1997) The concept of effective stress for soil, concrete and rock. Géotechnique 47(1):61–78
146. Lambe TW, Whitman RV (1969) Soil mechanics. Wiley, New York, 553pp
147. Lamé G (1852) Leçons sur la théorie mathématique de l'élasticité des corps solides (Lectures on the mathematical theory of elasticity of solid bodies). Bachelier, Paris, 335pp
148. Langguth HR, Treskatis C (1989) Reverse water level fluctuations in semiconfined aquifer systems – "Rhade effect". J Hydrol 109(1–2):79–93
149. Legarth B, Huenges E, Zimmermann G (2005) Hydraulic fracturing in a sedimentary geothermal reservoir: results and implications. Int J Rock Mech Mining Sci 42(7–8):1028–1041
150. Lehmann J (2007) Bio-energy in the black. Front Ecol Environ 5(7):381–387
151. Lin SJ, Jan KM, Weinbaum S, Chien S (1989) Transendothelial transport of low-density lipoprotein in association with cell mitosis in rat aorta. Arterioscler Thromb Vasc Biol 9(2):230–236
152. Liu PLF (1973) Damping of water waves over porous bed. J Hydraul Div ASCE 99(HY12):2263–2271
153. Logan TL, Mavor MJ, Khodaverdian M (1993) Western cretaceous coal seam project. Q Rev Methane Coal Seam Technol 10(April):6–12
154. Lu GQ, Zhao XS (eds)(2004) Nanoporous materials: science and engineering. Imperial College Press, London, 897pp
155. Mackenzie JK (1950) The elastic constants of a solid containing spherical holes. Proc Phys Soc Lond Sect B 63(361):2–11
156. Madsen OS (1978) Wave-induced pore pressures and effective stresses in a porous bed. Géotechnique 28(4):377–393
157. Magda W (1997) Wave-induced uplift force on a submarine pipeline buried in a compressible seabed. Ocean Eng 24(6):551–576

158. Mak AFT, Huang LD, Wang QQ (1994) A biphasic poroelastic analysis of the plow dependent subcutaneous tissue pressure and compaction due to epidermal loadings—issues in pressure sore. J Biomech Eng ASME 116(4):421–429
159. Mallard HH, Dalrymple RA (1977) Water waves propagating over a deformable bottom. In: 9th offshore technology conference, Houston, pp 141–146
160. Mandel J (1953) Consolidation des sols (etude mathematique) (Consolidation of soils (mathematical study)). Géotechnique 3:287–299
161. Martner S, Sparks N (1959) The electroseismic effect. Geophysics 24(2):297–308
162. Masoero E, Del Gado E, Pellenq RJM, Yip S, Ulm F-J (2014) Nano-scale mechanics of colloidal C-S-H gels. Soft Matter 10(3):491–499
163. Mavor MJ, Logan TL (1994) Recent advances in coal gas-well openhole well completion technology. J Pet Technol 46(7):587–593
164. Mehrabian A, Abousleiman Y (2011) General solutions to poroviscoelastic model of hydrocephalic human brain tissue. J Theor Biol 291:105–118
165. Mei CC, Foda MA (1981) Wave-induced responses in a fluid-filled poro-elastic solid with a free surface—a boundary layer theory. Geophys J R Astron Soc 66(3):597–631
166. Meinzer OE (1928) Compressibility and elasticity of artisan aquifers. Econ Geol 23:263–291
167. Melchior PJ (1983) The tides of the planet Earth, 2nd edn. Pergamon, Oxford/New York, 653pp
168. Mikhailov OV, Queen J, Toksöz MN (2000) Using borehole electroseismic measurements to detect and characterize fractured (permeable) zones. Geophysics 65(4):1098–1112
169. Millham NP, Howes BL (1995) A comparison of methods to determine *K* in a shallow coastal aquifer. Ground Water 33:49–57
170. Mow VC, Holmes MH, Lai WM (1984) Fluid transport and mechanical properties of articular cartilage—a review. J Biomech 17(5):377–394
171. Mow VC, Kuei SC, Lai WM, Armstrong CG (1980) Biphasic creep and stress relaxation of articular cartilage in compression—theory and experiments. J Biomech Eng ASME 102(1):73–84
172. Mu YK, Cheng AHD, Badiey M, Bennett R (1999) Water wave driven seepage in sediment and parameter inversion based on pore pressure data. Int J Numer Anal Methods Geomech 23(13):1655–1674
173. Murdoch LC, Chen J-L (1997) Effects of conductive fractures during *in-situ* electroosmosis. J Hazard Mater 55(1–3):239–262
174. Narasimhan TN (2005) Hydrogeology in North America: past and future. Hydrogeol J 13(1):7–24
175. Nierode DE (1985) Comparison of hydraulic fracture design methods to observed field results. J Pet Technol 37(11): 1831–1839
176. Norris A (1992) On the correspondence between poroelasticity and thermoelasticity. J Appl Phys 71(3):1138–1141
177. Nowacki W (1986) Thermoelasticity, 2nd edn. Pergamon, Oxford/New York, 566pp
178. Nur A, Booker JR (1972) Aftershocks caused by pore fluid flow? Science 175(4024):885–887
179. Oka M, Noguchi T, Kumar P, Ikeuchi K, Yamamuro T, Hyon SH, Ikada Y (1990) Development of an artificial articular cartilage. Clin Mater 6(4):361–381
180. Oka M, Ushio K, Kumar P, Ikeuchi K, Hyon SH, Nakamura T, Fujita H (2000) Development of artificial articular cartilage. Proc Inst Mech Eng Part H J Eng Med 214(1):59–68
181. Palmer AC, Rice JR (1973) Growth of slip surfaces in progressive failure of over-consolidated clay. Proc R Soc Lond Ser A Math Phys Eng Sci 332(1591):527–548
182. Paterson L (1986) A model for outbursts in coal. Int J Rock Mech Mining Sci 23(4):327–332
183. Paul P, Zoback M (2008) Wellbore stability study for the SAFOD borehole through the San Andreas Fault. SPE Drill Complet 23(4):394–408
184. Pearson C (1981) The relationship between microseismicity and high pore pressures during hydraulic stimulation experiments in low permeability granitic rocks. J Geophys Res 86(B9):7855–7864

185. Pennington WD, Davis SD, Carlson SM, Dupree J, Ewing TE (1986) The evolution of seismic barriers and asperities caused by the depressuring of fault planes in oil and gas fields of South Texas. Bull Seismol Soc Am 76(4):939–948
186. Phan LT (2008) Pore pressure and explosive spalling in concrete. Mater Struct 41(10):1623–1632
187. Phillips WS, House LS, Fehler MC (1997) Detailed joint structure in a geothermal reservoir from studies of induced microearthquake clusters. J Geophys Res Solid Earth 102(B6):11745–11763
188. Pinder, G. F., J. D. Bredehoeft, and H. H. Cooper (1969), Determination of aquifer diffusivity from aquifer response to fluctuations in river stage. Water Resour Res 5(4):850–855
189. Plumb RA, Cox JW (1987) Stress directions in eastern North America determined to 4.5 km from borehole elongation measurements. J Geophys Res Solid Earth Planets 92(B6):4805–4816
190. Poland JF (ed)(1984) Guidebook to studies of land subsidence due to ground-water withdrawal. UNESCO, Paris, 305pp
191. Polzer S, Gasser T, Markert B, Bursa J, Skacel P (2012) Impact of poroelasticity of intraluminal thrombus on wall stress of abdominal aortic aneurysms. BioMed Eng OnLine 11(1):1–13
192. Pratt WE, Johnson DW (1926) Local subsidence of the Goose Creek oil field. J Geol 34(7):577–590
193. Precht E, Huettel M (2004) Rapid wave-driven advective pore water exchange in a permeable coastal sediment. J Sea Res 51(2):93–107
194. Pride S (1994) Governing equations for the coupled electromagnetics and acoustics of porous media. Phys Rev B 50(21):15678–15696
195. Putnam JA (1949) Loss of wave energy due to percolation in a permeable sea bottom. Trans Am Geophys Union 30:349–356
196. Rahman MK, Naseby D, Rahman SS (2000) Borehole collapse analysis incorporating time-dependent pore pressure due to mud penetration in shales. J Pet Sci Eng 28(1–2):13–31
197. Raman-Nair W, Sabin GCW (1991) Wave-induced failure of poroelastic seabed slopes—a boundary element study. Proc Inst Civil Eng Part 2 Res Theory 91:771–794
198. Rappleye HS (1933) Recent areal subsidence found in releveling. Eng News Rec 110:845
199. Reid RO, Kajuira K (1957) On the damping of gravity waves over a permeable seabed. Trans Am Geophys Union 30:662–666
200. Rendulic L (1936) Porenziffer und porenwasserdruck in tonen (Void ratio and pore pressure in clays). Der Bauing 17:559–564
201. Revil A, Mahardika H (2013) Coupled hydromechanical and electromagnetic disturbances in unsaturated porous materials. Water Resour Res 49(2):744–766
202. Rice JR, Rudnicki JW (1979) Earthquake precursory effects due to pore fluid stabilization of a weakening fault zone. J Geophys Res 84(NB5):2177–2193
203. Rice JR, Simons DA (1976) Stabilization of spreading shear faults by coupled deformation-diffusion effects in fluid-infiltrated porous materials. J Geophys Res 81(29):5322–5334
204. Robinson TW (1939) Earth-tides shown by fluctuations of water-levels in wells in New Mexico and Iowa. Trans Am Geophys Union 20:656–666
205. Rodrigues JD (1983) The Noordbergum effect and characterization of aquitards at the Rio-Maior mining project. Ground Water 21(2):200–207
206. Roeloffs EA (1988) Fault stability changes induced beneath a reservoir with cyclic variations in water level. J Geophys Res Solid Earth Planets 93(B3):2107–2124
207. Rojstaczer S (1988) Determination of fluid flow properties from the response of water levels in wells to atmospheric loading. Water Resour Res 24(11):1927–1938
208. Rowe RK (2005) Long-term performance of contaminant barrier systems. Géotechnique 55(9):631–677
209. Rubey WW, Hubbert MK (1959) Role of fluid pressure in mechanics of overthrust faulting. 2. Overthrust belt in geosynclinal area of Western Wyoming in light of fluid-pressure hypothesis. Geol Soc Am Bull 70(2):167–205

210. Sakai T, Hatanaka K, Mase H (1992) Wave-induced effective stress in seabed and its momentary liquefaction. J Waterw Port Coast Ocean Eng ASCE 118(2):202–206
211. Schiffman RL, Chen AT-F, Jordan JC (1969) An analysis of consolidation theories. J Soil Mech Found Div ASCE 95(SM1):285–312
212. Schofield AN (2005) Disturbed soil properties and geotechnical design. Telford, London, 216pp
213. Schofield AN, Wroth CP (1968) Critical state soil mechanics. McGraw-Hill, New York, 310pp
214. Scott PP, Bearden WG, Howard GC (1953) Rock rupture as affected by fluid properties. Trans Am Inst Mining Metall Eng 198:111–124
215. Seed HB, Rahman MS (1978) Wave-induced pore pressure in relation to ocean-floor stability of cohesionless soils. Marine Geotechnol 3(2):123–150
216. Segall P (1989) Earthquakes triggered by fluid extraction. Geology 17(10):942–946
217. Segall P, Fitzgerald SD (1998) A note on induced stress changes in hydrocarbon and geothermal reservoirs. Tectonophysics 289(1–3):117–128
218. Segall P, Rice JR (1995) Dilatancy, compaction, and slip instability of a fluid-infiltrated fault. J Geophys Res Solid Earth 100(B11):22155–22171
219. Setton LA, Zhu WB, Mow VC (1993) The biphasic poroviscoelastic behavior of articular cartilage—role of the surface zone in governing the compressive behavior. J Biomech 26(4–5):581–592
220. Shapiro SA (2015) Fluid-induced seismicity. Cambridge University Press, Cambridge, 289pp
221. Siegrist RL, Lowe KS, Murdoch LC, Case TL, Pickering DA (1999) In situ oxidation by fracture emplaced reactive solids. J Environ Eng ASCE 125(5):429–440
222. Siffert RS, Luo GM, Cowin SC, Kaufman JJ (1996) Dynamic relationships of trabecular bone density, architecture, and strength in a computational model of osteopenia. Bone 18(2):197–206
223. Simon BR, Wu JSS, Carlton MW, Evans JH, Kazarian LE (1985) Structural models for human spinal motion segments based on a poroelastic view of the intervertebral disk. J Biomech Eng ASME 107(4):327–335
224. Simons DA (1977) Boundary-layer analysis of propagating mode II cracks in porous elastic media. J Mech Phys Solids 25(2):99–115
225. Simpson DW (1976) Seismicity changes associated with reservoir loading. Eng Geol 10(2–4):123–150
226. Skempton AW (1954) The pore pressure coefficients A and B. Géotechnique 4(4):143–147
227. Skempton AW (1960) Terzaghi's discovery of effective stress. In: Bjerrum L, Casagrande A, Peck RB, Skempton AW (eds) From theory to practice in soil mechanics. Wiley, New York, pp 42–53
228. Smith MB (1985) Stimulation design for short, precise hydraulic fractures. Soc Pet Eng J 25(3):371–379
229. Soltanzadeh H, Hawkes CD (2009) Assessing fault reactivation tendency within and surrounding porous reservoirs during fluid production or injection. Int J Rock Mech Mining Sci 46(1):1–7
230. Speziale S, Tenti G, Sivaloganathan S (2008) A poroelastic model of transcapillary flow in normal tissue. Microvasc Res 75(2):285–295
231. Šuklje L (1969) Rheological aspects of soil mechanics. Wiley Interscience, London/New York, 571pp
232. Teatini P, Castelletto N, Ferronato M, Gambolati G, Tosi L (2011) A new hydrogeologic model to predict anthropogenic uplift of Venice. Water Resour Res 47:W12507
233. Tennis PD, Jennings HM (2000) A model for two types of calcium silicate hydrate in the microstructure of Portland cement pastes. Cem Concr Res 30(6):855–863
234. Terzaghi K (1923) Die Berechnung der Durchlässigkeitsziffer des Tones aus dem Verlauf der hydrodynamischen Spannungserscheinungen (A method of calculating the permeability of clay from the history of hydrodynamic stress variation). Sitzungsber d Akad d Wiss Wien Math-Naturwiss Kl Abt IIa 132(3/4):125–138

235. Terzaghi K (1925) Erdbaumechanik auf Bodenphysikalischer Grundlage (Soil Mechanics on Soil Physical Basis). F. Deuticke, Leipzig u. Wien, 399pp
236. Terzaghi K (1936) The shearing resistance of saturated soils and the angle between the planes of shear. In: First international conference on soil mechanics, vol 1. Harvard University, Cambridge, pp 54–56
237. Terzaghi K (1943) Theoretical soil mechanics. Wiley, New York, 528pp
238. Terzaghi K, Peck RB (1948) Soil mechanics in engineering practice. Wiley, New York, 566pp
239. Terzaghi K, Peck RB, Mesri G (1996) Soil mechanics in engineering practice, 3rd edn. Wiley, New York, 592pp
240. Teufel LW (1983) Determination of *in-situ* stress from anelastic strain recovery measurements of oriented core, SPE 11649, SPE/DOE low permeability gas reservoirs symposium, Denver
241. Theis CV (1939) Earth tides as shown by fluctuations of water level in artesian wells in New Mexico. International Union of Geodesy and Geophysics, Washington Assembly, 11pp
242. Thimus JF, Abousleiman Y, Cheng AHD, Coussy O, Detournay E (eds)(1998) Poromechanics–a tribute to Maurice A. Biot. Balkema, Rotterdam/Brookfield, 648pp
243. Thompson A, Gist G (1993) Geophysical applications of electrokinetic conversion. Leading Edge 12(12):1169–1173
244. Thompson AH, Hornbostel S, Burns J, Murray T, Raschke R, Wride J, McCammon P, Sumner J, Haake G, Bixby M, Ross W, White BS, Zhou M, Peczak P (2007) Field tests of electroseismic hydrocarbon detection. Geophysics 72(1):N1–N9
245. Thompson R (1936) The seismic electric effect. Geophysics 1(3):327–335
246. Timoshenko SP, Goodier JN (1970) Theory of elasticity, 3rd edn. McGraw-Hill, New York, 567pp
247. Todd DK (1980) Groundwater hydrology, 2nd edn. Wiley, New York, 535pp
248. Ulm FJ, Constantinides G, Heukamp FH (2004) Is concrete a poromechanics material?—a multiscale investigation of poroelastic properties. Mater Struct 37(265):43–58
249. Vaccari A (1999) Clays and catalysis: a promising future. Appl Clay Sci 14(4):161–198
250. Valkó P, Economides MJ (1995) Hydraulic fracture mechanics. Wiley, Chichester, 318pp
251. Vandamme M, Ulm FJ (2013) Nanoindentation investigation of creep properties of calcium silicate hydrates. Cem Concr Res 52:38–52
252. van der Kamp G, Gale JE (1983) Theory of Earth tide and barometric effects in porous formations with compressible grains. Water Resour Res 19(2):538–544
253. van Eyden WAA, Kuper HW, Santema PW (1963) Some methods used in the geohydrological survey of the south-western deltaic area in the Netherlands. Proc Gen Assem Berkeley IUGG Int Assoc Sci Hydro Publ No 63:528–557
254. van Oort E, Hale AH, Mody FK, Roy S (1996) Transport in shales and the design of improved water-based shale drilling fluids. SPE Drill Complet 11(3):137–146
255. Verruijt A (1965) Discussion. In: Proceedings, sixth international conference on soil mechanics and foundation engineering, vol 3, Montreal, pp 401–402
256. Verruijt A (1969) Elastic storage of aquifers. In: DeWiest RJM (ed) Flow through porous media. Academic, New York, pp 331–376
257. Vito RP, Dixon SA (2003) Blood vessel constitutive models—1995–2002. Ann Rev Biomed Eng 5:413–439
258. Voight B (1968) Determination of the virgin state of stress in the vicinity of a borehole from measurements of a partial anelastic strain tensor in drill cores. Felsmech und Ing 6:201–215
259. Warpinski NR, Teufel LW (1989) A viscoelastic constitutive model for determining *in-situ* stress magnitudes from anelastic strain recovery of core. SPE Prod Eng 4(3):274–279
260. Warpinski NR, Teufel LW (1989) Author's reply to Discussion of "A viscoelastic constitutive model for determining *in-situ* stress magnitudes from anelastic strain recovery of core". SPE Prod Eng 4(3):287–289
261. Weinbaum S, Cowin SC, Zeng Y (1994) A model for the excitation of osteocytes by mechanical loading-induced bone fluid shear stresses. J Biomech 27(3):339–360
262. Wolff RG (1970) Relationship between horizontal strain near a well and reverse water level fluctuation. Water Resour Res 6(6):1721–1728

263. Wong TF, David C, Zhu WL (1997) The transition from brittle faulting to cataclastic flow in porous sandstones: mechanical deformation. J Geophys Res Solid Earth 102(B2):3009–3025
264. Wu JZ, Dong RG, Rakheja S, Schopper AW, Smutz WP (2004) A structural fingertip model for simulating of the biomechanics of tactile sensation. Med Eng Phys 26(2):165–175
265. Yamamoto T, Koning HL, Sellmeijer H, Van Hijum E (1978) On the response of a poro-elastic bed to water waves. J Fluid Mech 87:193–206
266. Yang J, Jiang GL (2003) Experimental study on properties of pervious concrete pavement materials. Cem Concr Res 33(3):381–386
267. Yang M, Taber LA, Clark EB (1994) A nonlinear poroelastic model for the trabecular embryonic heart. J Biomech Eng ASME 116(2):213–223
268. Yerkes RF, Castle RO (1976) Seismicity and faulting attributable to fluid extraction. Eng Geol 10(2–4):151–167
269. Yew CH (1997) Mechanics of hydraulic fracturing. Gulf Professional Publishing, Houston, 182pp
270. Yin L, Elliott DM (2004) A biphasic and transversely isotropic mechanical model for tendon: application to mouse tail fascicles in uniaxial tension. J Biomech 37(6):907–916
271. Yin S (2013) Numerical analysis of thermal fracturing in subsurface cold water injection by finite element methods. Int J Numer Anal Methods Geomech 37(15):2523–2538
272. Yin S, Dusseault MB, Rothenburg L (2007) Analytical and numerical analysis of pressure drawdown in a poroelastic reservoir with complete overburden effect considered. Adv Water Resour 30(5):1160–1167
273. Young A (1913) Tidal phenomena at inland boreholes near Craddock. Trans R Soc South Afr 31:61–106
274. Zhang DJ, Weinbaum S, Cowin SC (1998) On the calculation of bone pore water pressure due to mechanical loading. Int J Solids Struct 35(34–35):4981–4997
275. Zhao YS, Hu YQ, Wei JP, Yang D (2003) The experimental approach to effective stress law of coal mass by effect of methane. Transp Porous Media 53(3):235–244
276. Zheng ZQ, Kemeny J, Cook NGW (1989) Analysis of borehole breakouts. J Geophys Res Solid Earth Planets 94(B6):7171–7182
277. Zhu Z, Toksöz M (2005) Seismoelectric and seismomagnetic measurements in fractured borehole models. Geophysics 70(4):F45–F51
278. Zoback MD, Moos D, Mastin L, Anderson RN (1985) Well bore breakouts and *in situ* stress. J Geophys Res 90(B7):5523–5530

http://www.springer.com/978-3-319-25200-1

Poroelasticity
Cheng, A.H.-D.
2016, XXVI, 877 p. 171 illus., 62 illus. in color.,
Hardcover
ISBN: 978-3-319-25200-1